Presenting a global riverine microplastic transport model based on mechanical principles

Arthur Ronner
Master thesis
MSc Industrial Ecology
Leiden University | TU Delft

Delft
August 3, 2024
Supervisors: Dr. V. Barbarossa
Dr. J. Mogollón
Dr. N. Navarre

Presenting a global riverine microplastic transport model based on mechanical principles

Summary

Recently, there has been more and more research on the abundance of MPs (MPs) in oceans, seas, and rivers. A lot is still uncertain about the distribution of MPs, and whether they are mainly deposited in seas & oceans, or river sediments. As global models on MP transport through rivers have only used statistical methods, we present a global riverine MP transport model based on mechanical principles. The model incorporates particle advection, settling, entrainment, and input emissions from wastewater treatment plants. The model was run for a period of 5 years, on 8 MP mixes of 15 MPs each, with the same 24 uncertainty scenarios for each MP mix (totalling 192 runs). Exported (to seas and oceans) and sedimented MPs showed a linear increase over time, while MPs suspended in the river reached steady state, but showed heavy seasonal fluctuations. Under the modelled uncertainties, after 5 years of simulation time, 76% of MPs are exported to seas and oceans and 19 % of MPs are deposited in river sediment. 5% of MPs were suspended in the water column. Major contributing areas to global MP emissions are area's with large population densities, like Europe, North America, China & South East Asia, and India. Our work contributes to the understanding of MP flows through rivers, and could be used as a starting point for a MP material flow analysis, or as the basis for MP impact assessments. Future iterations of the model should implement man-made barriers and reservoirs, which were not considered in the current version of the model.

1. Introduction

Microplastics (MPs), plastics smaller than 5mm, are more and more present everywhere on the globe due to the continuous use of plastics in all sectors of society (Browne, 2015; Koutnik et al., 2021). Because of their small size, they are easily consumed by (micro) organisms, and have entered the (human) food chain (Du and Wang, 2021; Mamun et al., 2023; Toussaint et al., 2019). Following this wide spread of MPs, their negative impact on ecosystems and public health is becoming increasingly apparent, and includes neurotoxicity in marine life, and organ damage and cancers in humans (Du and Wang, 2021; Eze et al., 2024; Karbalaei et al., 2018). This omnipresence of MPs raises the question of how MPs are transported from human emission sources to the environment. Air and water transport have been listed as the two main means of transportation (Koutnik et al., 2021). In recent years, the MP contents in the earths freshwater and oceans has received increased attention (2021; Meijer et al., 2021; Zong et al., 2024). Microplastics can originate from primary (directly produced) or secondary (macroplastic degradation) sources (Chamas et al., 2020). Examles include synthetic clothing (Belzagui et al., 2019; Stone et al., 2020; Volgare et al., 2021), tire wear (Vogelsang et al., 2018), cosmetics (Napper et al., 2015; Q. Sun et al., 2020), and industrial processes (Ngo et al., 2019). If we focus on the river network, one of the main sources of MPs are wastewater treatment plants (WWTPs) (Liu et al., 2021; Ngo et al., 2019; Sadia et al., 2022). Even though they filter domestic waste, a small percentage of MPs is still present in the excreted wastewater, resulting in recorded daily WWTP MP emission rates in the order of 10^6 to 10^9 particles per WWTP (Azizi et al., 2022; J. Sun et al., 2019). This range varies heavily between WWTP plants and depends on everything from WWTP size, population served, as well as WWTP removal technique and study methodology (Gao et al., 2023; Iyare et al., 2020). Due to the difficulty in detecting MPs, modelling approaches can greatly aid our understanding of MP transport (Kooi et al., 2018). There have been numerous studies on the fate of MPs that reach the river network. The focus of studies ranges from a single river (Arbeloa and Marzadri, 2024; Besseling et al., 2017; Daily and Hoffman, 2020; Mennekes and Nowack, 2023; Nizzetto et al., 2016), to a continental or global scale (Drummond et al., 2022; Mai et al., 2020; Meijer et al., 2021; Quik et al., 2023; Strokal et al., 2023; van Wijnen et al., 2019). Larger scale studies employ statistical methods, while smaller river scale studies use statistical methods, mechanistic, or mixed methods (Uzun et al., 2022). However, to the best of our knowledge, a global approach that uses mechanistic processes to model MP flows through river networks has yet to be proposed.

Here we bridge this gap by introducing a global riverine MP transport model. Our model simulates the river transport of different types of MPs emitted by WWTPs around the globe, using transportational methods from Lazar et al. (2010); Nizzetto et al. (2016); Yu et al. (2022), on a 5 arcmin scale (10 km near at the equator). The MP accumulation in different stocks (river sediment, river suspension, and exported) are subsequently tested under different uncertainty conditions. With this model, we aim to aid global estimates of MP accumulation, and to scope which factors impact MP accumulation in river sediment, versus exported MPs globally. This model outline leads to the following research question:

> ***RQ:*** *How can a global model for riverine microplastic transport using transportational mechanisms aid our understanding of mi-*

croplastic deposition in river sediment and seas & oceans?

2. Method

The method section is threefold. First, we discuss the model outline. This includes the different transportation flows implemented, and MP mix handling. Second, we discuss the model implementation. This includes the models hydrological background, and flow prioritisation. Lastly, we describe the uncertainty analysis methodology, including the uncertainty sampling, as well as the MP mix selection.

2.1. Model outline

The proposed model subdivides MPs into particle classes (particles with similar properties). For each MP class, its transport across the globe is modelled, given advection, emission, settling, and entrainment flows. The model functions in discrete time and space. It subdivides the globe into given latitude and longitude cells. Subsequently, flows between compartments are modelled for every time step, for homogeneously mixed river water and river sediment segments. A small scale schematic overview of the model is presented in figure 2.

2.2. Model flows

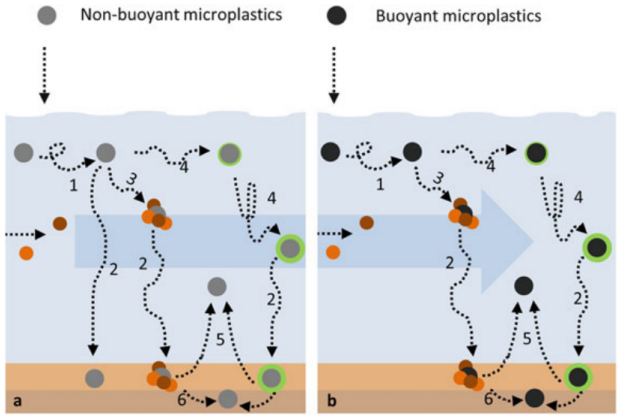

Figure 1: Transporting processes of non-buoyant (a) and buoyant microplastics (b). Processes include (1) turbulent transport, (2) settling, (3) aggregation, (4) biofouling, (5) entrainment, and (6) burial. From Kooi et al. (2018)

Phenomena that influence MP transport through rivers are shown in figure 1. Buoyant particles have been assumed to accumulate enough biofouling such that they immediately exhibit non-buoyant behaviour (Kooi and Koelmans, 2019). Further effects of biofouling have been disregarded in the modelling flows, but are instead considered in the density distributions of particles. Moreover, the effects of aggregation, and burial have been disregarded. The model flows are defined below for one grid cell.

2.2.1. Advection

River flow is represented in this model using advection. The number of advected MPs is given by formula 1.

$$N_{MP,A} = Q(t)t_s\frac{N_{MPsus}}{V} \tag{1}$$

Where $N_{MP,A}$ is the amount of MPs advected from a river segment in one model time step, Q (m^3/s) is the river segment discharge at time t, t_s is the duration of a model time step in seconds, N_{MPsus} is the number of MP suspended in the segments water column, and V (m^3) is the river segment volume. The river volume is calculated assuming the river is rectangular ($L \cdot W \cdot H$). Each timestep, $N_{MP,A}$ is subtracted from its source cell, and added to its downstream target cell.

2.2.2. WWTPs Emissions

We estimate MP emissions from WWTPs, ignoring other emission sources. This choice was made because of both the importance of WWTPs as a MP source, and the availability of a global WWTPs dataset by Macedo et al. (2022). In future studies, these inputs could be extended to include other input flows, such as landfill leaching and road dust particles. If we focus on WWTPs, Ngo et al. (2019) mentions different pathways of MPs to WWTPS, where domestic streams are the most prominent. The global WWTPs dataset from Macedo et al. (2022) includes data for daily wastewater discharge and population served per WWTP. We use the population served parameter as a proxy to the number of MPs emitted for different plants (Ayankunle et al., 2023). This approach was chosen because MP fibers constitute the largest fraction of MP emissions, and are emitted due to domestic washing (J. Sun et al., 2019). Based on available data, we then derive the following formula for MP emissions from a given WWTP.

$$N_{MP,E} = \frac{r_{eff}}{p_{MPF}} N_{MPF,wash}\frac{P_{served}}{s_{hh}} \cdot \frac{n_{w,hh}}{t}(p_{wm} + (1 - p_{wm})f_{hw}) \tag{2}$$

Where $N_{MP,E}$ is the number of MP particles discharged by the WWTPs per day, r_{eff} is the removal efficiency of the WWTP, and p_{MPF} is the percentage of microplastic fibers of the total MP emissions. $N_{MPF,wash}$ is the amount of MP fibers emitted per wash, P_{served} is the population served by the WWTP, s_{hh} is the average household size (of the WWTPs country), $n_{w,hh}$ is the amount of washes done a household per day (dependent on household size), and t is one time step of the model, in days. Lastly, p_{wm} is the percent of the population that owns a washing machine (per country), and f_{hw} is the difference between emissions of a washing machine cycle and a handwash. The source and derivation of each of these

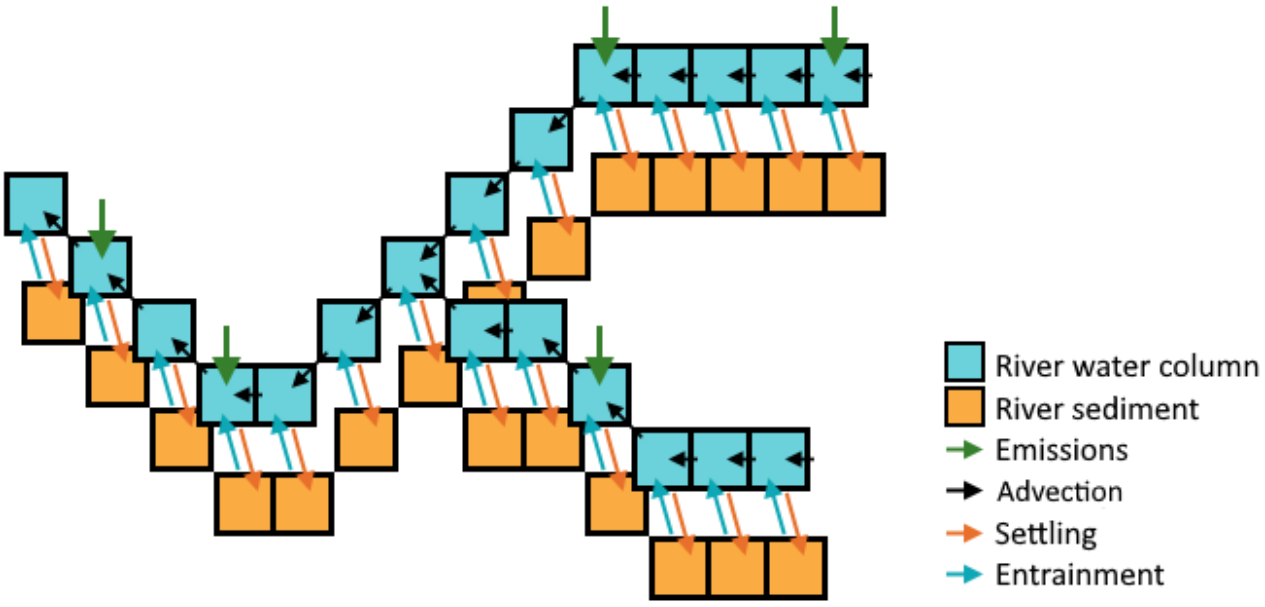

Figure 2: Schematic representation of the model for a small river. Each timestep, MP from each river segment advect to one adjacent segment (black arrows), emissions are added to respective water columns (green arrows), and settling (red arrows) and entrainment flows (blue arrows) occur between the respective water column and sediment segments.

Table 1: Source and methodology details for each of the variables used in equation 2.

Name	Symbol	Source	Details
Removal efficiency	r_{eff}	Azizi et al. (2022)	Statistical analysis of MP removal efficiencies of different WWTPs types (primary, secondary, and advanced).
Percent of MP fibers in WWTP output	p_{MPF}	J. Sun et al. (2019)	Relative occurrence of MP fibers in relation to other types of MP particles, based on a literature review. Full results shown in figure 3.
MP fiber particles per wash	$N_{MPF,wash}$	Belzagui et al. (2019); Kruschwitz et al. (2014); (2023)	Standard washing load of 4.08 kg (Kruschwitz et al., 2014), 65.1 % of synthetic fibers ("Materials Market Report", 2023), 175-560 MP fibers released per g of synthetic clothes (Belzagui et al., 2019).
Number of washes per household	$N_{wash,hh}$	Pakula and Stamminger (2010)	For households of sizes <2.2, between 2.2 and 2.7 and >2.7, the number of washes per year is equal to 150, 165, and 177, respectively.
Percent of washing machine ownership	p_{wm}	Laitala et al. (2018)	Nearest neighbor approximation ($k = 5$) based on a washing machine ownership dataset (Laitala et al., 2018), and countries HDI (result shown in figure B.1). HDI data included in Appendix A.
Average household size	s_{hh}	United Nations Population Division	Per country. In combination with national census data when required. Data can be found in the model repository (Appendix A).
Handwash emission factor	f_{hw}	Wang et al. (2023)	A handwash emits 7.8 % of the MP fibers of a normal washing cycle of the same clothes. We disregard differences in emitted fiber lengths.

variables is given table 1. With this formula, an MP emission can be derived for each of the different WWTPs in our dataset. When multiple MP types are used, the $N_{MP,E}$ will be distributed among the different MP types.

2.2.3. Gravitational settling

There have been numerous studies on the settling velocity of MPs. While earlier works describe all MP particles as spherical (Nizzetto et al., 2016), more recent laboratory studies estimated settling velocity of MPs based on particles properties (Goral et al., 2023; Kaiser et al., 2019; Waldschläger and Schüttrumpf, 2019; Yu et al., 2022). The works of Goral et al. (2023); Kaiser et al. (2019); Waldschläger and Schüttrumpf (2019) all derive drag coefficients, while Yu et al. (2022) derives a settling velocity directly. The gravitational settling methodology for the model is based on the works Yu et al. (2022), as the direct settling velocity estimation, based on particle shape, size, and density, can be straightforwardly implemented in the model. After the settling velocity w_s (m/s) is determined (equation 4), the number of MP that settle from a river water column to its sediment segment, N_{settle}, is given by equation 3.

$$N_{settle} = w_s \frac{N_{MPsus}}{V} LWt_s \tag{3}$$

Where N_{MPsus} is the amount of MPs suspended in the segments water column, V (m^3) the river volume, and L(m) and W(m) the river length and bankfull width, respectively.

Settling velocity The formula for w_s, and its required components, are given in equation 4.

$$w_s = \sqrt[3]{\mu(T) g \frac{\rho_s - \rho_f}{\rho_f}} \sqrt{\frac{4 d_*}{3 C_d}} \tag{4a}$$

$$d_* = \sqrt[3]{\frac{(\rho_s - \rho_f) g}{\rho_f \mu(T)^2}} d_n, \tag{4b}$$

$$C_d = \frac{C_{d,s}}{\left(d_*^{\beta_1} \psi^{d_*^{\beta_2}} CSF^{d_*^{\beta_3}} \right)^{\beta_4}}, \tag{4c}$$

$$C_{d,s} = \frac{432}{d_*^3} \left(1 + 0.022 d_*^3\right)^{0.54} + 0.47 \left[1 - \exp\left(-0.15 d_*^{0.45}\right)\right], \tag{4d}$$

Where d_* is the dimensionless particle diameter, C_d is the drag coefficient, d_n(m)$(= \sqrt[3]{6V_p/\pi})$ is the diameter of the volume equivalent sphere, and V_p(m^3) is the particle volume. $C_{d,s}$ the drag law for spherical particles, ψ and CSF are particle sphericity and Corey shape factor, as defined in section 2.3. $\beta_1, \beta_2, \beta_3$, and β_4 are scaling parameters that are fixed for one model run. The 95% confidence intervals for these parameters are shown in table 3. The water viscosity of segments is calculated by using the viscosity tables provided by Wagner and Kretzschmar (2008), through a lookup table method, with a granularity of 2 °C. This look up table is included in the model repository (Appendix A).

2.2.4. Entrainment

Entrainment is incorporated in the model with equation 5, first introduced by Lazar et al. (2010) for sediment dynamics, later adapted for MPs by Nizzetto et al. (2016).

$$N_{ent} = \gamma_8 N_{MPsed} P_{prop} \Omega f \tag{5a}$$

$$P_{prop} = \min(\max(\frac{a_{max} - a_{low}}{a_{upp} - a_{low}}, 0), 1) \tag{5b}$$

$$a_{max} = 9.9941 (w^*)^{2.5208} \tag{5c}$$

$$w^* = \sqrt{g H \gamma_7 s} \tag{5d}$$

$$\Omega = \rho_f g \frac{Q}{WH} s \tag{5e}$$

$$f = \frac{R}{R_{max}} = \frac{HW/(2H+W)}{\pi(W/2)^2/(\pi W)} \tag{5f}$$

Where N_{ent} is the number of entrained particles, N_{MPsed} the number of particles in the sediment segment, and P_{prop} is the fraction of MPs that can entrain, based on the maximum particle entrainment diameter a_{max}, and the MP category lower and upper diameter bounds a_{low} and a_{upp}. These are 90 % and 110 % of the particles a in the model, respectively. The particle diameter a corresponds to the particles largest dimension for non spherical particles. w^* is the river shear velocity, Ω is the stream power per unit area of riverbed, and s(m/m) is the river slope. f is the friction factor, relating the hydraulic radius R to the maximum hydraulic radius of a pipe (R_{max}). γ_7 and γ_8 are scaling parameters that represent the spatial variation in the hydromorphological characteristics (Lazar et al., 2010). Equation 5, and especially P_{prop}, is based on spherical particles.

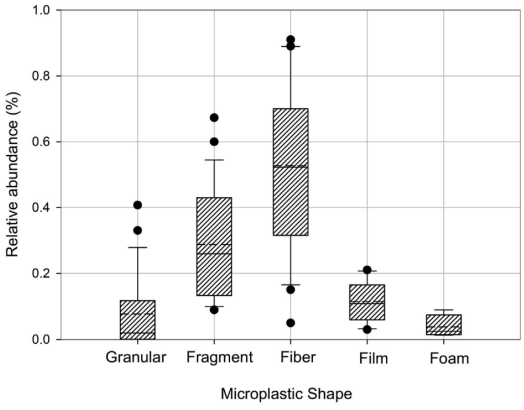

Figure 3: Relative abundance of MP particle types in WWTP discharge. The median, 10th, 25th, 75th and 90th percentiles were plotted as vertical boxes with error bars. The dots indicate outliers, and the dashed lines refer to the average. From J. Sun et al. (2019).

2.3. Microplastic mix

MPs come in various shapes, densities, and sizes (J. Sun et al., 2019). Generally, studies divide MPs in five distinct categories: Fibers (lines), fragments, beads (pellets), foams, and films (sheets) (Kooi and Koelmans, 2019; Niari et al., 2023). Generally, fibers and fragments are most common throughout the environment (Burns and Boxall, 2018; J. Sun et al., 2019). The relative distribution of different MP categories in WWTPs emissions can be found in figure 3.

Particles size, density and shape impact its settling and transport characteristics in a river (Goral et al., 2023). Particle shape can be described using a number of different metrics (Han et al., 2023; Kooi and Koelmans, 2019; Yu et al., 2022). Two frequently used measures for particle shape are particle sphericity ψ (Chien, 1994), and the Corey Shape Factor CSF (Corey et al., 1949). Their respective formulas are found in equations 6 and 7.

$$\psi = \frac{A_{sph}}{A_s} = \frac{4\pi \frac{d_n}{2}^2}{A_s} \tag{6}$$

Where $d_n(\mathrm{m})(= \sqrt[3]{6V_p/\pi})$ is the diameter of the volume equivalent sphere, and $V_p(\mathrm{m}^3)$ is the particle volume. Note that $\psi \in (0, 1]$, as the surface area of the volume equivalent sphere minimises a particles surface area. As $\psi \to 1$, a particle is more and more spherical. However, sphericity alone has trouble representing particles with a complex surface area. For instance, MP fish line and MP pellets might have the same sphericity, while having different settling properties (Khatmullina and Isachenko, 2017). Thus, the Corey shape factor was used as another method of quantifying particle shape (Corey et al., 1949).

$$CSF = \frac{a}{\sqrt{bc}} \tag{7}$$

Where a, b, and c are the particle dimensions chosen in such a way that $a \geq b \geq c$. The CSF is a measure of the similarity between the different dimensions of a particle. A fiber for instance, will have a very low shape factor.

Multiple types of microplastics were considered in the model, to account for different settling and entrainment interactions. We select a sample of microplastics per model run. This mix is constructed by choosing 3 distinct MPs within each of the five major MP categories (fibers, fragments, foams, films, and beads). Then, the properties of each of these 15 microplastics are chosen using Latin Hypercube sampling (McKay et al., 1979). The ranges and variables considered for the chosen MP mixes are given in table 2. Fragments, foams, and films are each modelled as cuboids. Fibers and beads are modelled as cylinders and ellipsoids, respectively. After the different particles are selected, the relative occurrences of different MPs within one MP category are calculated based on the particles shape, size, and density. This is done by following the work of Kooi and Koelmans (2019), which is outlined in Appendix C.

Table 2: Upper and lower ranges of each of the five microplastic types. b and c are expressed as a fraction of a and b, respectively.

Name	Lower	Upper	Unit
Fiber a	5.0×10^{-5}	1.0×10^{-3}	m
Fiber b	1.0×10^{-3}	0.5	-
Fiber ρ	1000	1290	kg
Fragment a	5.0×10^{-5}	1.0×10^{-3}	m
Fragment b	0.1	1	-
Fragment c	0.1	1	-
Fragment ρ	1000	1810	kg
Foam a	5.0×10^{-5}	1.0×10^{-3}	m
Foam b	0.1	1	-
Foam c	0.1	1	-
Foam ρ	1000	1180	kg
Bead a	5.0×10^{-5}	1.0×10^{-3}	m
Bead b	0.6	1	-
Bead c	0	1	-
Bead ρ	1000	1810	kg
Film a	5.0×10^{-5}	1.0×10^{-3}	m
Film b	0.1	1	-
Film c	0.01	0.1	-
Film ρ	1000	1810	kg

2.4. Model implementation

Our model relies on hydrological characteristics of rivers globally. To this end, we utilized the futurestreams dataset (Bosmans et al., 2022), which based upon PCR-GLOBWB 2 (Sutanudjaja et al., 2018) and DynaWat (Wanders et al., 2019), computes rasterised (at 5-arcmin resolution) river discharge and water temperature over time. PCR-GLOBWB 2 is a grid-based global hydrology and water resources model, at a 5-arcmin (10km at the equator) resolution. DynWat is a global dynamical 1-D water energy routing model, that solves both the energy and water balance, to simulate river temperatures. Similar to PCR-GLOBWB 2, DynWat operates at a 5 arcmin resolution.

Our model used the same 5×5 arcmin resolution as the futurestreams dataset. During model runs, advection, settling, and entrainment calculations are each performed on rasterised MP stocks. Alterations of equations 1-5 can be found in Appendix E. In the current implementation of the model, the effect of dams and reservoirs on river flow rate have been disregarded.

Emissions As our emissions input is constant over time, it is calculated once at the start of a model run. For each of the grid cells in our model, equation 8 is used to calculate its total emissions per timestep.

$$E_{MP,i,j} = \sum_{w=1}^{W} N_{MPw} r_{w,i,j}, \qquad r_{w,i,j} \in \{0, 1\} \tag{8}$$

Where i, j represent the grid cells latitude and longitude coordinate, respectively. W is the number of WWTPs. $r_{w,i,j}$ is 1, if WWTP w's discharge output is located in grid cell i, j, and is 0 otherwise.

Model flow prioritisation As four different flows alter the MP stocks each time step, we preserved mass balance in the model using flow prioritisation. This procedure is shown in equation 9. Where N_n and N_o are the new and old stocks, respectively. fn is the n^{th} flow of the model. The order of flows used was the following: advection → emissions → settling → entrainment.

$$\begin{aligned} N_n = & N_o - \max(\min(f_1, N_o), 0) \\ & - \max(\min(f_2, N_o - f_1), 0) \\ & - ... \\ & - \max(\min(f_n, N_o - f_1 - f_2 - ... - f_{n-1}), 0) \end{aligned} \tag{9}$$

2.5. Uncertainty analysis

Because of the uncertainty in the formulation of the model, we employ Latin hypercube sampling (McKay et al., 1979), to represent the full uncertainty space. The uncertainties considered in the model, as well as their value ranges are given in table 3. This results in the following total uncertainty analysis design (see figure 4). For the WWTPs MP fractions, the resultant values from a given sample should sum up to one. To accomplish this, the generated samples are subsequently fitted to a Dirichlet distribution (Connor and Mosimann, 1969).

We ran the model for a combined total of 192 times. These 192 ($= 24 \times 8$) runs are constructed by generating an uncertainty sample of size 24, and 8 different generated MP mixes of 15 MPs each. These MP mixes can be found in Appendix G. For each mix, the same uncertainty sample (table G.1) was used, to establish comparable results. Furthermore, the model was ran over a 5 year period, using input data from futurestreams from January 1st 1996 - December 31st 2000. Data was saved at quarterly (91 day) intervals, resulting in a total of 20 recorded timesteps. All data produced by the model is stored in the netCDF4 format. The total abundance of MPs, in number of particles, is subsequently analysed for the river water column (suspended), river sediment, and exported (sea/ocean) stocks. The definition of these three stocks is shown in equation 10. Where i, j represent the latitude and longitude coordinates of N, and ϕ_{ij} the direction of flow at that particular coordinate (where 1 represents bottom left, and 9 top right), where 5 signifies no flow. i, j sum over the region of interest.

$$N_{sus} = \sum_{ij} N_{MPsus,ij} \quad \text{if} \quad \phi_{ij} \neq 5 \tag{10a}$$

$$N_{sed} = \sum_{ij} N_{MPsed,ij} \quad \text{if} \quad \phi_{ij} \neq 5 \tag{10b}$$

$$N_{exp} = \sum_{ij} N_{MPsus,ij} + N_{MPsed,ij} \quad \text{if} \quad \phi_{ij} = 5 \tag{10c}$$

The region of interest can be the whole globe, or a smaller hydrological unit. The chosen watersheds in the results correspond to the ones used in the futurestreams parallelisation methodology (Bosmans et al., 2022).

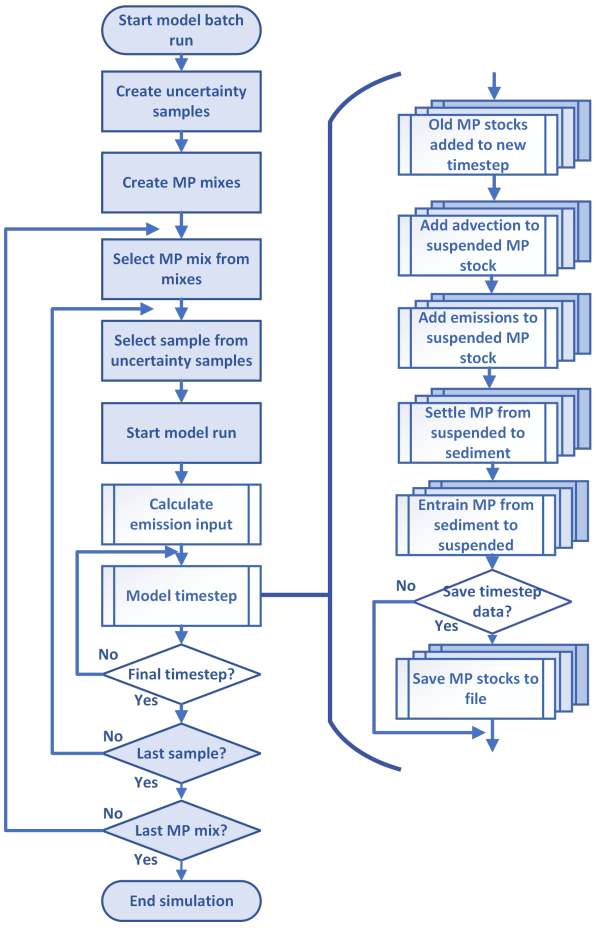

Figure 4: Flowchart for the uncertainty analysis of the model. Uncertainty analysis steps are shown in light blue, and processes belonging to a model run are shown in white. Multiple boxes indicate that this process is executed for each of the MPs used in the model.

2.5.1. partial correlation analysis

To scope the impact of the different uncertainties in the model, we performed a semi-partial Pearson correlation test between the uncertainties and the outcomes of the model (Kim, 2015). This test measures the degree of association between x and y, after removing the effect of one or more controlling variables. In this analysis, we assumed that the model outcomes are dependent on all of

Table 3: Model uncertainties and their ranges, as used for the model uncertainty sampling. After sampling, WWTPs MP fractions are subsequently fitted to a Dirichlet distribution, to sum up to one.

name	Symbol	lower	upper	default	Unit	Source
a7	γ_7	8.0×10^{-5}	0.08	4.0×10^{-2}	-	Lazar et al., 2010
a8	γ_8	2.0×10^{-7}	4.0×10^{-6}	2.1×10^{-6}	s^2kg^{-1}	2010
Beta 1	β_1	-0.36	-0.13	-0.25	-	Yu et al., 2022
Beta 2	β_2	-0.34	0.4	0.03	-	2022
Beta 3	β_3	0.16	0.49	0.33	-	2022
Beta 4	β_4	0.12	0.37	0.25	-	2022
WWTPs r_{eff} primary	r_{eff}	0.766	0.881	0.833	-	Azizi et al., 2022
WWTPs r_{eff} secondary	r_{eff}	0.938	0.966	0.955	-	2022
WWTPs r_{eff} advanced	r_{eff}	0.987	0.9955	0.9922	-	2022
Microplastics per wash	$N_{MPF,wash}$	465 000	1 487 000	976 000	N	Belzagui et al., 2019
WWTPs fiber fraction	p_{MPfib}	0.32	0.68	0.527	-	J. Sun et al., 2019
WWTPs fragment fraction	p_{MPfra}	0.15	0.43	0.20	-	2019
WWTPs film fraction	p_{MPfil}	0.08	0.17	0.1	-	2019
WWTPs bead fraction	p_{MPb}	0	0.12	0.02	-	2019
WWTPs foam fraction	p_{MPfo}	0.02	0.07	0.03	-	2019

the model uncertainties. Prior to running the test, we first normalised all uncertainties and outcomes of the model.

3. Results

The results will first consider global microplastic accumulation over time, and the influence of different MP mixes on these results. Then, spatial differences in the stocks will be considered, followed by an uncertainty correlation analysis. A note on the model performance can be found in Appendix F.

3.1. Global microplastic accumulation

We first consider the mean total MP accumulation over time per stock type across 24 runs for different MP mixes (figure 5). The respective coefficients of variation (variance divided by mean) are given in figure 6.

Although there are stark differences between mixes when we consider the suspended and sediment stocks, the relative influence of the three stocks is similar across the 8 mixes. Under the given uncertainty conditions, the mean accumulated exported stocks (2×10^{16}) are greater than the other stocks (5×10^{15} sedimented, 1.2×10^{15} suspended) by at least a factor of 4 after 5 years of model runtime. This signifies that the travel time to seas and rivers is, in general, lower than the settling time for an average particle. Next to particle and stream properties, this could be in part because of the locations of WWTPs (see figure D.1), as a large portion of the plants is located close to seas and oceans (near densely populated areas). If we consider the suspended stocks, we observe that these are lower than the sedimented stocks for all mixes. This entails that the settling dynamics outweigh the particles entrainment. Mix 3 shows a smaller sedimented fraction than other mixes.

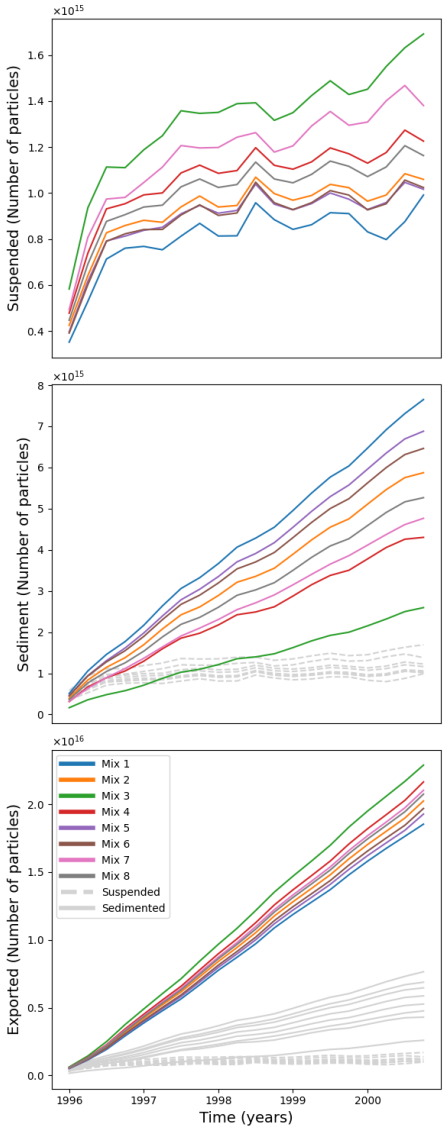

Figure 5: Mean global accumulated MPs across 24 runs per stock type, per MP mix, in number of MPs. Smaller stocks are added in grey is subsequent plots for comparison. Y axes are different between plots.

Moreover, the number of particles suspended in rivers is the most prone to seasonal fluctuations, and has only a very minor increase after the initial 2 years of runtime. The sedimented and exported stocks however, both show a linear increase that exceeds the suspended stock in all of our 8 means. The sedimented MP stock shows heavy variation between mixes, where mix 1 and mix 3 differ by a factor 4 after 5 years of runtime. As the total number of MPs emitted is the same across the mixes, we observe an anti correlation between a high sediment stock, and a high exported and suspended stock within one mix. Another finding of our model is that the global MP content in river water is constant, except for seasonal fluctuations. This could be due to seasonal fluctuations in river discharge, which impacts the amount of exported MPs.

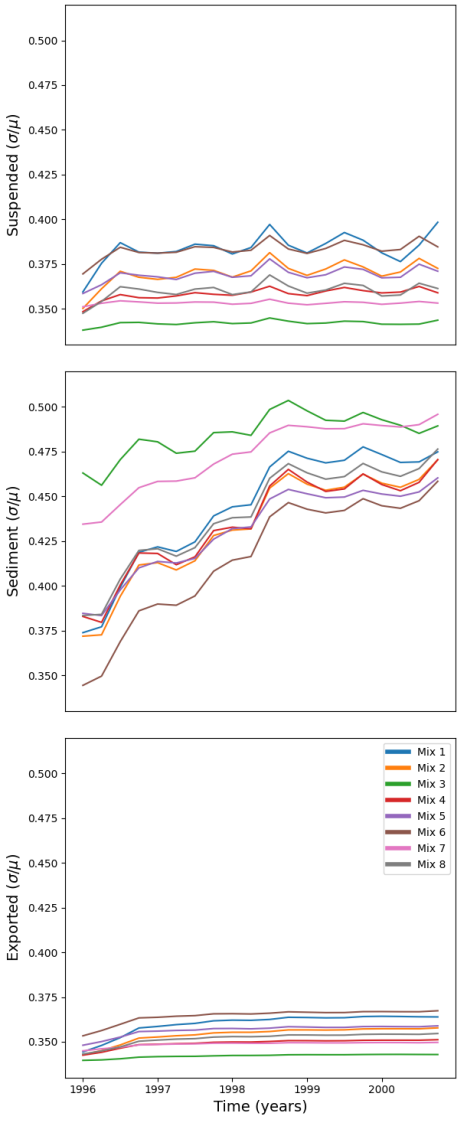

Figure 6: Coefficient of variation of global accumulated MPs across 24 runs per stock type, per MP mix.

The coefficient of variation (CV) across 24 runs, is shown in figure 6. Firstly, CVs found are consistent with the finding that exported stocks are larger than sedimented stocks. For all mixes except for mix 3, the sedimented stocks are higher than the suspend stocks within one standard deviation. For mix 3, this assertion is less certain. If we examine the differences between CV of the different stock types, the sedimented stocks have a higher CV, which also equalises at a later stage compared to suspended and exported stocks. This indicates that the rate of sedimentation is more dependent on the different uncertainties in the model than the other two stocks. The delayed equalisation time could also relate to the initial uncertainty in the different emission conditions.

The sizes of the largest dimension of particles in different MP mixes, and their relative occurrence, are given in figure 7. Mix 3,4 and 7, which reported the lowest mean rate of sedimentation, contain significantly smaller MP fibers (the most occurring type of MP) compared to other mixes. These fibers also constitute 80-99% of the fibers in their respective mix. For mix 3, the same holds for its fragments composition (the second most occurring type of MP). This is consistent with previous studies, as for instance Nizzetto et al. (2016) also notes that for smaller MPs, there is significantly less sediment retention. Conversely, mix 1, with the highest sedimentation rate, also contains a high concentration of larger fibers.

3.2. Spatial patterns

The MP accumulation in watersheds globally is represented in figure 9. This figure shows mean accumulation after 5 years across all 192 runs for total MP abundance. Figure 9 also shows the MP distribution across stocks. Watersheds correspond to the ones used in the futurestreams parallelisation methodology (Bosmans et al., 2022). Major contributing watersheds can be found in densely populated areas, like Europe, North America, China & South East Asia, and India. A lot of the major watersheds share similar distribution trends compared to the global means. However, some watersheds show stark differences. For instance, the sedimented and exported stock in the India-Pakistan watershed are almost equal. We observe the same stock distribution in the watersheds of Uzbekistan-Turkmenistan, and to a lesser degree in the West Coast of the US & Mexico. Moreover, island watersheds, like Indonesia & Papua New Guinea, New Zealand, Japan and Iceland, show a relatively high exported fraction, due to their relatively small land area.

The spatial coefficient of variation for the different stock types is given in figure 10. Here, both exported and total MP emissions have a relatively constant CV or 0.3 globally. This entails that for those stocks, the uncertainty in the output is proportional to the mean output. However, suspended and sedimented stocks show heavier fluctuations. Sparsely populated polar climate areas show the heaviest sediment fluctuations, with a CV between 1-1.65. For suspended MPs, the West Coast the US

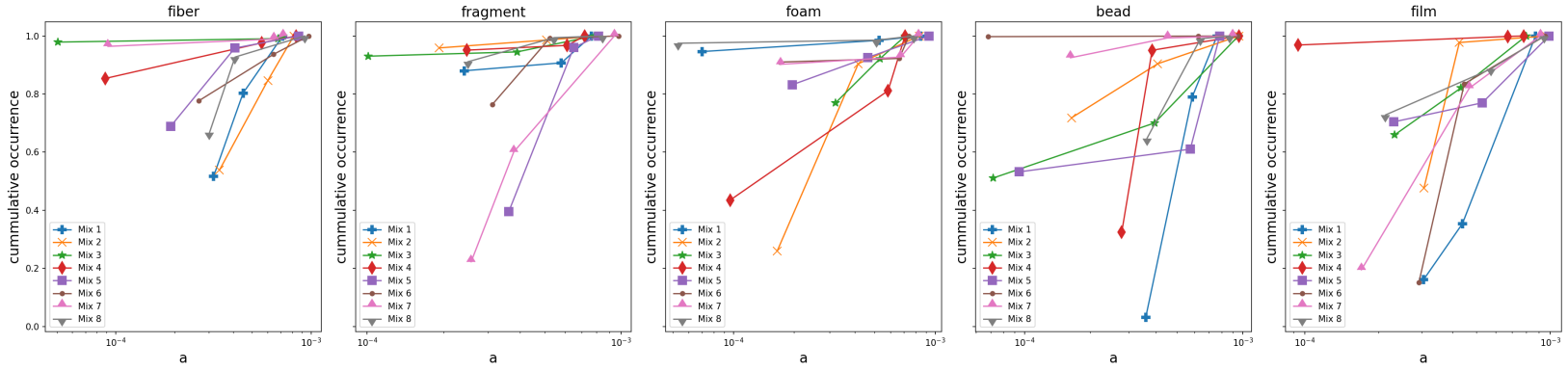

Figure 7: Different microplastic mixes characteristics. Particle sizes versus cumulative occurrence, per particle category.

and Mexico, West Australia, and the previously identified India-Pakistan and Uzbekistan-Turkmenistan watersheds show fluctuations of 0.6-0.9 CV.

3.3. Uncertainty analysis

The different uncertainties and their impact on the model are shown in figure 8. This figure shows semi-partial Pearson correlation between different model outcomes and model uncertainties. Both WWTPs $N_{MP,wash}$ and WWTPs r_{eff} secondary are correlated with all of the outcomes. This could be because both of these uncertainties directly impact the input of MPs globally. As secondary WWTPs are far more common than primary or advanced WWTPs, this result is expected. However, the sedimented stocks are correlated to a lesser degree, and so is the secondary r_{eff} for the suspended stock. For the sedimented stock, this could be explained by its larger CV compared to the other stocks, which makes direct correlation harder to establish. Overall, figure 8 shows that the sedimented stock is weakly correlated to roughly the same degree for 5 uncertainties. The sediment stock is also the only outcome that is correlated with one of the WWTPs MP fractions. This could be due to its dependence on smaller fibers, as we have seen previously in figure 5.

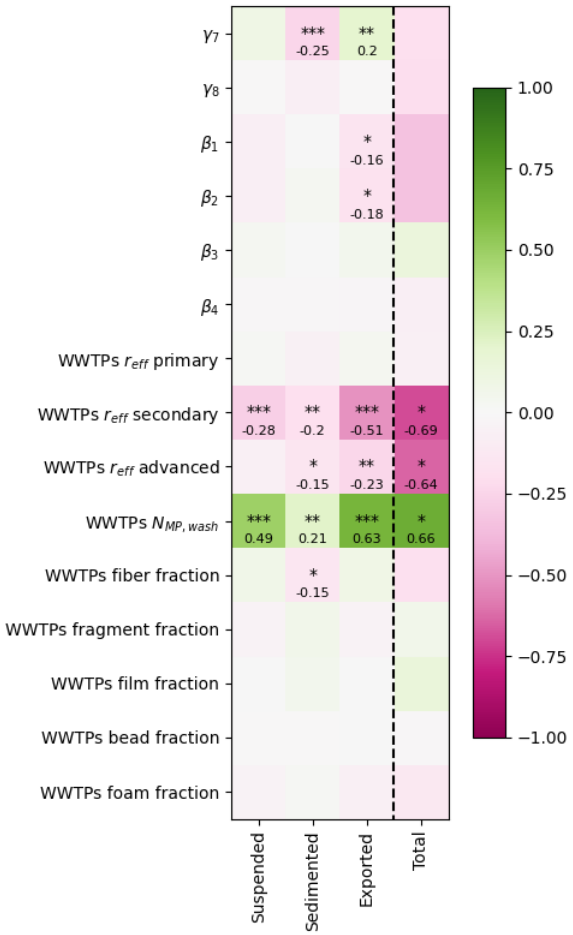

Figure 8: Partial correlation between uncertainties and the four outcomes. The results for total MP are across 24 runs, the other stocks are over the 192 runs. Stars indicate a p value of <0.05, more stars indicates an even smaller p. The squares with relevant p have their partial correlation value listed.

4. Discussion

The distribution of MPs throughout the earths water system has been area of debate in recent years (Mennekes and Nowack, 2023; Strokal et al., 2023). While at first research was focused on marine MPs, recently freshwater has gained more and more attention (Range et al., 2023). There is still much debate about the fate of riverine MPs, and if they end in freshwater or in oceans. With this work we aim to contribute to this discussion. The global accumulation results in this study suggests that deposition rates to seas and oceans outweigh those to river sediments by a factor 4.

This is contrary to findings in literature, where different studies report that rivers might be a major sink for MPs (2023). Some studies, like Mennekes and Nowack (2023), note that lakes and reservoirs are a big candidate for MP retention. As our model excludes the worlds lakes and reservoirs, our relatively large fraction of oceanic

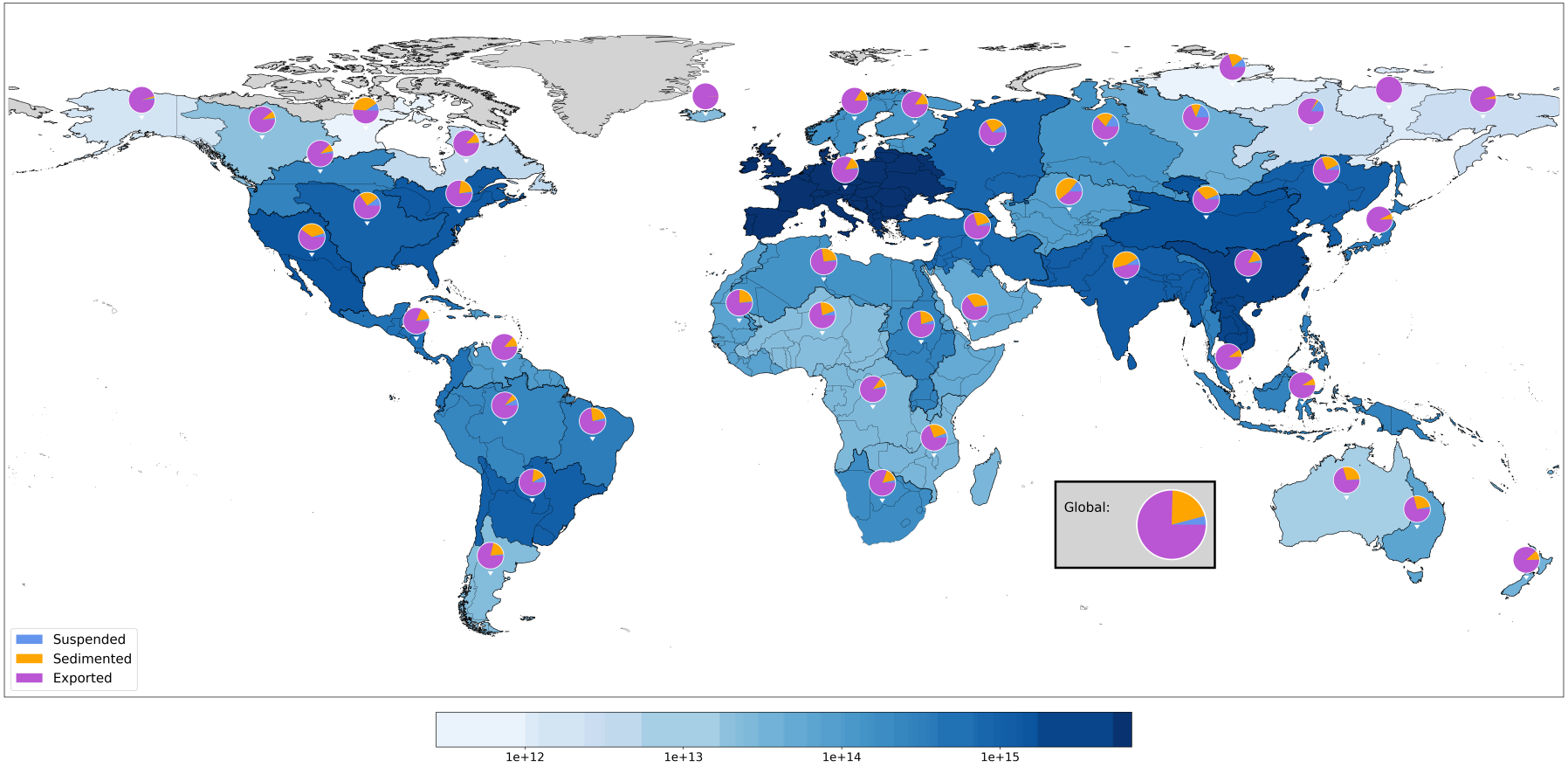

Figure 9: Mean total MP accumulation after 5 years over 192 runs, in number of particles. Pie charts indicate the relative contribution of different stock types.

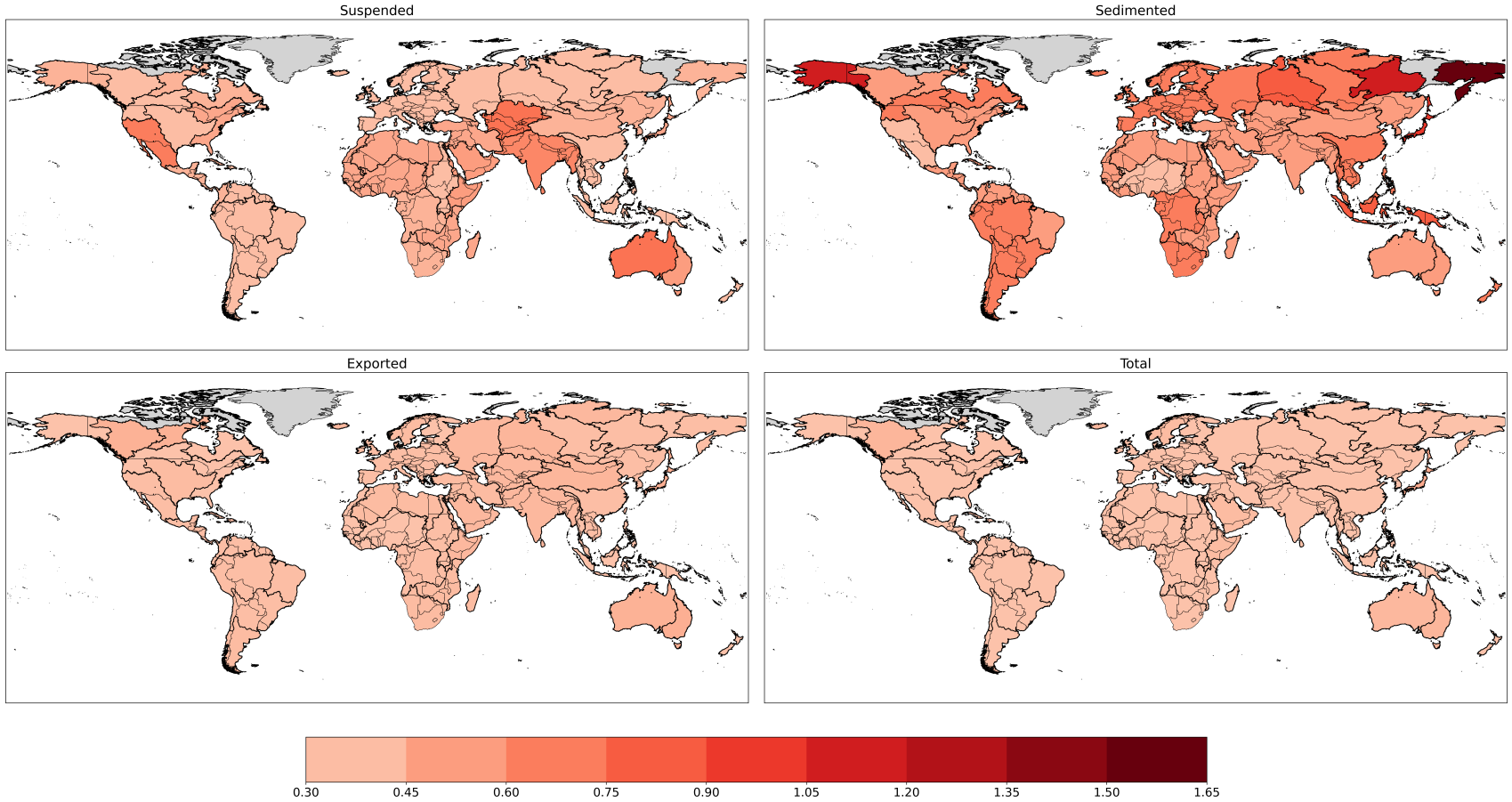

Figure 10: The spatial coefficient of variation (σ/μ) per stock over 192 runs. Different plots show different stock types (shown in their title).

transport could be partially explained due to this simplification. Moreover, Drummond et al. (2020) also note that hyporheic exchange, the interaction between river stream and sediment, can potentially retain MPs for a longer period of time, especially for particles $<100\,\mu$m. Finally, the exclusion of sources other than WWTPs could limit the spatial distribution of MPs to be centered around large urbanised areas, which are often located near coastlines ("National Aggregates of Geospatial Data Collection: Population, Landscape, And Climate Estimates", 2012). Still, the presented model offers a unique insight, as it is the first work to incorporate mechanistic principles in a global riverine MP model. It should be noted that the presented accumulation rates over 5 years do not directly translate to ecosystem impact, due to the shear volume difference between freshwater bodies and seas & oceans. Still, our model can be used as a starting point for a global material flow analysis method for MPs, or as the starting point for an impact assessment on MPs worldwide.

Spatial patterns The spatially explicitness of our model can greatly aid our understanding of regional differences in riverine MP transport. Given the differences between watersheds, our research suggests that MP reduction policies should also consider the local climate and river characteristics to be most effective. Specifically, the difference in distribution of MP stocks between the India-Pakistan watershed and the global average is striking. This could be explained by the large accumulation of WWTPs in the proximity of New Dehli (figure D.1), which is far from any export locations, together with large seasonal variations and low flow conditions due to the dry climate. This could lead MPs to settle before they reach export locations. The Uzbekistan-Turkmenistan watershed, with a similar stock distribution, also has its major WWTPs located more land inward, and has similar climate conditions. Considering the CV of different watersheds, there are large outlies in cold regions for the sedimentation fractions. WWTPs in these areas are close to oceans, and as there are only very few WWTPs, different MP mixes or uncertainties in the settling velocity will have a relatively large impact on sedimentation rate, because of the low settling time period of particles. For the CV in suspended MP, the same India-Pakistan, Uzbekistan-Turkmenistan, and West coast USA- Mexico are outliers. One explanation for this phenomenon would be the relatively long rivers in these areas. This leads for a larger capacity for MPs, and therefor more room for fluctuations under different uncertainty conditions, especially given the seasonal variation in these areas.

Uncertainty analysis The uncertainty analysis for the sedimented stock entails that the interaction between different uncertainties plays a large role in the amount of sedimented MP. A larger sample size could shed more light on the relative impact of the 5 correlated uncertainties. Interestingly, the sedimented stock is not correlated with β_1-β_4, the uncertainties associated with particle settling. Conversely, the exported stock is weakly correlated with both γ_7 as well as β_1 & β_2, showing that both the entrainment and settling equations slightly impact the exported stocks.

Limitations Firstly, the MP emissions from WWTPs bear the burden of data availability. This is due to the complex differences between different WWTPs, population washing habits, as well as synthetic clothing use. While our current estimation tries to account for said factors, further studies are advised to update the emissions input based on new monitoring insights, especially regarding regional differences. Secondly, the advection flows in the model do not account for lakes, man-made barriers, and reservoirs. This could impact the retention rate of MPs in river sediment, due to the longer residence time in lakes and reservoirs. For the settling flow, the approximations of Yu et al. (2022) are based on empirical measurements for a Reynolds number < 100. However, due to the turbulent nature of rivers, this settling velocity might be impacted differently in different river types. Additionally, no direct method of quantifying the hyporheic exchange for MPs exists to date, which can impact retention rates in river sediments for particles $<100\,\mu$m. The entrainment equation as proposed by Lazar et al. (2010); Nizzetto et al. (2016) consider spherical particles, while our MP mixes are explicitly non-spherical. Based on our knowledge, no straightforward modelling strategy for the entrainment of non-spherical MPs exists to date. The channel characteristics (represented by uncertainty γ_8) can vary greatly between different rivers, but γ_8 was kept constant globally in this study.
Due to the general computational intensity of the model, the number of MP categories per run (15), as well as the number of uncertainty scenarios (24), is still relatively low. A larger uncertainty sample is advised to confirm the findings in from this project. Moreover, the relative MP occurrence from Kooi and Koelmans (2019) is based on riverine, as well as marine measurements. This could be a different occurrence distribution compared to WWTPs outflow.

5. Conclusion

There has been much debate about the role of river sediments versus seas & oceans as MP stocks. To aid this discussion, we present a global MP river transport model, that estimates riverine MP fate worldwide based on WWTPs MP emissions. Our model shows that worldwide, under almost all the considered uncertainty conditions, over a 5 year period, 76% of MPs are exported to seas and oceans, while the majority of the remaining MPs (19%) is deposited in river sediment. Exceptions are very small particles, which tend to get sedimented

less often. This could be an inaccuracy of only considering gravitational settling, and disregarding more complex river particle interactions, like hyporheic exchange (Drummond et al., 2020; 2022). Major contributing areas to global MP emissions are area's with large population densities, like Europe, North America, China & South East Asia, and India. In drier areas with large populations living land-inward, sedimentation can get about as prevalent as MP export. The CV for export and total stocks is relatively stable worldwide, at 0.3-0.45. For sedimentation, spatial CV outliers (at 1.35-1.65) are located in sparsely populated polar areas. For suspended stocks, CV outliers (at 0.75-0.9) are situated in dry environments. The most partially correlated uncertainties on all stocks are the WWTPs r_{eff} of secondary power plants, and the WWTPs $N_{MP,wash}$ parameters. The uncertainty influence on sedimented stocks is most split, having a weak correlation for 5 different parameters. The entrainment variable γ_7 is correlated weakly with both sediment and export stocks, while the settling variables β_1 and β_2 are only correlated weakly with exported stocks.

To improve the current version of the model, further research is advised to implement man-made reservoirs and barriers, as both can have a great influence on the retention of MPs. Furthermore, running a larger uncertainty sample and executing the model for a longer period of time is recommended, to confirm the current findings of the model.

New additions to this model could be to connect the model outcomes (a global, spatially explicit MP emission distribution) to human water and river sediment utilisation, or ecosystem activity, to scope health or environmental impacts of riverine MP pollution globally. Another addition is to connect the current exported MP information to an oceanic flow rate dataset (for instance ESR, 2009), to more properly scope MPs diffusion in seas and oceans , and which ecosystems might be impacted most.

References

Arbeloa, N. P. D., & Marzadri, A. (2024). Modeling the transport of microplastics along river networks. *Science of The Total Environment*, *911*, 168227. https://doi.org/10.1016/j.scitotenv.2023.168227

Ayankunle, A. Y., Buhhalko, N., Pachel, K., Lember, E., Kõrgmaa, V., Mishra, A., & Lind, K. (2023). Estimating microplastics related to laundry wash and personal care products released to wastewater in major estonian cities: A comparison of calculated and measured microplastics. *Journal of Environmental Health Science and Engineering*, *21*, 225–237. https://doi.org/10.1007/s40201-023-00856-z

Azizi, N., Nasseri, S., Nodehi, R. N., Jaafarzadeh, N., & Pirsaheb, M. (2022). Evaluation of conventional wastewater treatment plants efficiency to remove microplastics in terms of abundance, size, shape, and type: A systematic review and meta-analysis. *Marine Pollution Bulletin*, *177*, 113462. https://doi.org/10.1016/j.marpolbul.2022.113462

Belzagui, F., Crespi, M., Álvarez, A., Gutiérrez-Bouzán, C., & Vilaseca, M. (2019). Microplastics' emissions: Microfibers' detachment from textile garments. *Environmental Pollution*, *248*, 1028–1035. https://doi.org/10.1016/j.envpol.2019.02.059

Besseling, E., Quik, J. T., Sun, M., & Koelmans, A. A. (2017). Fate of nano- and microplastic in freshwater systems: A modeling study. *Environmental Pollution*, *220*, 540–548. https://doi.org/10.1016/j.envpol.2016.10.001

Bosmans, J., Wanders, N., Bierkens, M. F. P., Huijbregts, M. A. J., Schipper, A. M., & Barbarossa, V. (2022). Futurestreams, a global dataset of future streamflow and water temperature. *Scientific Data*, *9*, 307. https://doi.org/10.1038/s41597-022-01410-6

Browne, M. A. (2015). Sources and pathways of microplastics to habitats. Springer International Publishing. https://doi.org/10.1007/978-3-319-16510-3_9

Burns, E. E., & Boxall, A. B. (2018). Microplastics in the aquatic environment: Evidence for or against adverse impacts and major knowledge gaps. *Environmental Toxicology and Chemistry*, *37*, 2776–2796. https://doi.org/10.1002/etc.4268

Chamas, A., Moon, H., Zheng, J., Qiu, Y., Tabassum, T., Jang, J. H., Abu-Omar, M., Scott, S. L., & Suh, S. (2020). Degradation rates of plastics in the environment. *ACS Sustainable Chemistry & Engineering*, *8*, 3494–3511. https://doi.org/10.1021/acssuschemeng.9b06635

Chien, S.-F. (1994). Settling velocity of irregularly shaped particles. *SPE Drilling & Completion*, *9*, 281–289. https://doi.org/10.2118/26121-PA

Connor, R. J., & Mosimann, J. E. (1969). Concepts of independence for proportions with a generalization of the dirichlet distribution. *Journal of the American Statistical Association*, *64*, 194–206. https://doi.org/10.1080/01621459.1969.10500963

Corey, A. T., Albertson, M. L., Fults, J. L., Rollins, R. L., Gardner, R. A., Klinger, B., Bock, R. O., et al. (1949). Influence of shape on the fall velocity of sand grains.

Daily, J., & Hoffman, M. J. (2020). Modeling the three-dimensional transport and distribution of multiple microplastic polymer types in lake erie. *Marine Pollution Bulletin*, *154*, 111024. https://doi.org/10.1016/j.marpolbul.2020.111024

Drummond, J. D., Nel, H. A., Packman, A. I., & Krause, S. (2020). Significance of hyporheic exchange for predicting microplastic fate in rivers. *Environmental Science & Technology Letters*, *7*, 727–732. https://doi.org/10.1021/acs.estlett.0c00595

Drummond, J. D., Schneidewind, U., Li, A., Hoellein, T. J., Krause, S., & Packman, A. I. (2022). Microplastic accumulation in riverbed sediment via hyporheic exchange from headwaters to mainstems. *Science Advances*, *8*. https://doi.org/10.1126/sciadv.abi9305

Du, H., & Wang, J. (2021). Characterization and environmental impacts of microplastics. *Gondwana Research*, *98*, 63–75. https://doi.org/10.1016/j.gr.2021.05.023

ESR. (2009). Oscar third degree resolution ocean surface currents. https://doi.org/10.5067/OSCAR-03D01

Eze, C. G., Nwankwo, C. E., Dey, S., Sundaramurthy, S., & Okeke, E. S. (2024). Food chain microplastics contamination and impact on human health: A review. *Environmental Chemistry Letters*. https://doi.org/10.1007/s10311-024-01734-2

Gao, Z., Chen, L., Cizdziel, J., & Huang, Y. (2023). Research progress on microplastics in wastewater treatment plants: A

holistic review. *Journal of Environmental Management*, *325*, 116411. https://doi.org/10.1016/j.jenvman.2022.116411

Goral, K. D., Guler, H. G., Larsen, B. E., Carstensen, S., Christensen, E. D., Kerpen, N. B., Schlurmann, T., & Fuhrman, D. R. (2023). Settling velocity of microplastic particles having regular and irregular shapes. *Environmental Research*, *228*, 115783. https://doi.org/10.1016/j.envres.2023.115783

Han, N., Ao, H., Mai, Z., Zhao, Q., & Wu, C. (2023). Characteristics of (micro)plastic transport in the upper reaches of the yangtze river. *Science of The Total Environment*, *855*, 158887. https://doi.org/10.1016/j.scitotenv.2022.158887

Iyare, P. U., Ouki, S. K., & Bond, T. (2020). Microplastics removal in wastewater treatment plants: A critical review. *Environmental Science: Water Research & Technology*, *6*, 2664–2675. https://doi.org/10.1039/D0EW00397B

Kaiser, D., Estelmann, A., Kowalski, N., Glockzin, M., & Waniek, J. J. (2019). Sinking velocity of sub-millimeter microplastic. *Marine Pollution Bulletin*, *139*, 214–220. https://doi.org/10.1016/j.marpolbul.2018.12.035

Karbalaei, S., Hanachi, P., Walker, T. R., & Cole, M. (2018). Occurrence, sources, human health impacts and mitigation of microplastic pollution. *Environmental Science and Pollution Research*, *25*, 36046–36063. https://doi.org/10.1007/s11356-018-3508-7

Karney, C. F. F. (2013). Algorithms for geodesics. *Journal of Geodesy*, *87*, 43–55. https://doi.org/10.1007/s00190-012-0578-z

Khatmullina, L., & Isachenko, I. (2017). Settling velocity of microplastic particles of regular shapes. *Marine Pollution Bulletin*, *114*, 871–880. https://doi.org/10.1016/j.marpolbul.2016.11.024

Kim, S. (2015). Ppcor: An r package for a fast calculation to semi-partial correlation coefficients. *Communications for Statistical Applications and Methods*, *22*, 665–674. https://doi.org/10.5351/CSAM.2015.22.6.665

Kooi, M., Besseling, E., Kroeze, C., van Wezel, A. P., & Koelmans, A. A. (2018). Modeling the fate and transport of plastic debris in freshwaters: Review and guidance. https://doi.org/10.1007/978-3-319-61615-5_7

Kooi, M., & Koelmans, A. A. (2019). Simplifying microplastic via continuous probability distributions for size, shape, and density. *Environmental Science & Technology Letters*, *6*, 551–557. https://doi.org/10.1021/acs.estlett.9b00379

Koutnik, V. S., Leonard, J., Alkidim, S., DePrima, F. J., Ravi, S., Hoek, E. M., & Mohanty, S. K. (2021). Distribution of microplastics in soil and freshwater environments: Global analysis and framework for transport modeling. *Environmental Pollution*, *274*, 116552. https://doi.org/10.1016/j.envpol.2021.116552

Kruschwitz, A., Karle, A., Schmitz, A., & Stamminger, R. (2014). Consumer laundry practices in germany. *International Journal of Consumer Studies*, *38*, 265–277. https://doi.org/10.1111/ijcs.12091

Laitala, K., Klepp, I. G., & Henry, B. (2018, February). Use phase of apparel: A literature review for life cycle assessment with focus on wool.

Lazar, A. N., Butterfield, D., Futter, M. N., Rankinen, K., Thouvenot-Korppoo, M., Jarritt, N., Lawrence, D. S., Wade, A. J., & Whitehead, P. G. (2010). An assessment of the fine sediment dynamics in an upland river system: Inca-sed modifications and implications for fisheries. *Science of The Total Environment*, *408*, 2555–2566. https://doi.org/10.1016/j.scitotenv.2010.02.030

Liu, W., Zhang, J., Liu, H., Guo, X., Zhang, X., Yao, X., Cao, Z., & Zhang, T. (2021). A review of the removal of microplastics in global wastewater treatment plants: Characteristics and mechanisms. *Environment International*, *146*, 106277. https://doi.org/10.1016/j.envint.2020.106277

Macedo, H. E., Lehner, B., Nicell, J., Grill, G., Li, J., Limtong, A., & Shakya, R. (2022). Distribution and characteristics of wastewater treatment plants within the global river network. *Earth System Science Data*, *14*, 559–577. https://doi.org/10.5194/essd-14-559-2022

Mai, L., Sun, X.-F., Xia, L.-L., Bao, L.-J., Liu, L.-Y., & Zeng, E. Y. (2020). Global riverine plastic outflows. *Environmental Science & Technology*, *54*, 10049–10056. https://doi.org/10.1021/acs.est.0c02273

Mamun, A. A., Prasetya, T. A. E., Dewi, I. R., & Ahmad, M. (2023). Microplastics in human food chains: Food becoming a threat to health safety. *Science of The Total Environment*, *858*, 159834. https://doi.org/10.1016/j.scitotenv.2022.159834

Materials market report. (2023, December).

McKay, M. D., Beckman, R. J., & Conover, W. J. (1979). Comparison of three methods for selecting values of input variables in the analysis of output from a computer code. *Technometrics*, *21*, 239–245. https://doi.org/10.1080/00401706.1979.10489755

Meijer, L. J. J., van Emmerik, T., van der Ent, R., Schmidt, C., & Lebreton, L. (2021). More than 1000 rivers account for 80% of global riverine plastic emissions into the ocean. *Science Advances*, *7*. https://doi.org/10.1126/sciadv.aaz5803

Mennekes, D., & Nowack, B. (2023). Predicting microplastic masses in river networks with high spatial resolution at country level. *Nature Water*, *1*, 523–533. https://doi.org/10.1038/s44221-023-00090-9

Napper, I. E., Bakir, A., Rowland, S. J., & Thompson, R. C. (2015). Characterisation, quantity and sorptive properties of microplastics extracted from cosmetics. *Marine Pollution Bulletin*, *99*, 178–185. https://doi.org/10.1016/j.marpolbul.2015.07.029

National aggregates of geospatial data collection: Population, landscape, and climate estimates. (2012). https://doi.org/10.7927/H4F769GP

Ngo, P. L., Pramanik, B. K., Shah, K., & Roychand, R. (2019). Pathway, classification and removal efficiency of microplastics in wastewater treatment plants. *Environmental Pollution*, *255*, 113326. https://doi.org/10.1016/j.envpol.2019.113326

Niari, M. H., Jaafarzadeh, N., Dobaradaran, S., Niri, M. V., & Dargahi, A. (2023). Release of microplastics to the environment through wastewater treatment plants: Study on four types of wastewater treatment processes. *Water, Air, & Soil Pollution*, *234*, 589. https://doi.org/10.1007/s11270-023-06594-0

Nizzetto, L., Bussi, G., Futter, M. N., Butterfield, D., & Whitehead, P. G. (2016). A theoretical assessment of microplastic transport in river catchments and their retention by soils and river sediments. *Environmental Science: Processes & Impacts*, *18*, 1050–1059. https://doi.org/10.1039/C6EM00206D

Pakula, C., & Stamminger, R. (2010). Electricity and water consumption for laundry washing by washing machine worldwide. *Energy Efficiency*, *3*, 365–382. https://doi.org/10.1007/s12053-009-9072-8

Quik, J., Meesters, J., & Koelmans, A. (2023). A multimedia model to estimate the environmental fate of microplastic particles. *Science of The Total Environment*, *882*, 163437. https://doi.org/10.1016/j.scitotenv.2023.163437

Range, D., Scherer, C., Stock, F., Ternes, T. A., & Hoffmann, T. O. (2023). Hydro-geomorphic perspectives on microplastic distribution in freshwater river systems: A critical review. *Water Research*, *245*, 120567. https://doi.org/10.1016/j.watres.2023.120567

Sadia, M., Mahmood, A., Ibrahim, M., Irshad, M. K., Quddusi, A. H. A., Bokhari, A., Mubashir, M., Chuah, L. F., & Show, P. L. (2022). Microplastics pollution from wastewater treatment plants: A critical review on challenges, detection, sustainable removal techniques and circular economy. *Environmental Technology & Innovation*, *28*, 102946. https://doi.org/10.1016/j.eti.2022.102946

Stone, C., Windsor, F. M., Munday, M., & Durance, I. (2020). Natural or synthetic – how global trends in textile usage threaten freshwater environments. *Science of The Total Environment*, *718*, 134689. https://doi.org/10.1016/j.scitotenv.2019.134689

Strokal, M., Vriend, P., Bak, M. P., Kroeze, C., van Wijnen, J., & van Emmerik, T. (2023). River export of macro- and microplastics to seas by sources worldwide. *Nature Communications*, *14*, 4842. https://doi.org/10.1038/s41467-023-40501-9

Sun, J., Dai, X., Wang, Q., van Loosdrecht, M. C., & Ni, B.-J. (2019). Microplastics in wastewater treatment plants: Detection, occurrence and removal. *Water Research*, *152*, 21–37. https://doi.org/10.1016/j.watres.2018.12.050

Sun, Q., Ren, S.-Y., & Ni, H.-G. (2020). Incidence of microplastics in personal care products: An appreciable part of plastic pollution. *Science of The Total Environment*, *742*, 140218. https://doi.org/10.1016/j.scitotenv.2020.140218

Sutanudjaja, E. H., van Beek, R., Wanders, N., Wada, Y., Bosmans, J. H. C., Drost, N., van der Ent, R. J., de Graaf, I. E. M., Hoch, J. M., de Jong, K., Karssenberg, D., López, P. L., Peßenteiner, S., Schmitz, O., Straatsma, M. W., Vannametee, E., Wisser, D., & Bierkens, M. F. P. (2018). Pcr-globwb 2: A 5 arcmin global hydrological and water resources model. *Geoscientific Model Development*, *11*, 2429–2453. https://doi.org/10.5194/gmd-11-2429-2018

Toussaint, B., Raffael, B., Angers-Loustau, A., Gilliland, D., Kestens, V., Petrillo, M., Rio-Echevarria, I. M., & den Eede, G. V. (2019). Review of micro- and nanoplastic contamination in the food chain. *Food Additives & Contaminants: Part A*, *36*, 639–673. https://doi.org/10.1080/19440049.2019.1583381

Uzun, P., Farazande, S., & Guven, B. (2022). Mathematical modeling of microplastic abundance, distribution, and transport in water environments: A review. *Chemosphere*, *288*, 132517. https://doi.org/10.1016/j.chemosphere.2021.132517

van Wijnen, J., Ragas, A. M., & Kroeze, C. (2019). Modelling global river export of microplastics to the marine environment: Sources and future trends. *Science of The Total Environment*, *673*, 392–401. https://doi.org/10.1016/j.scitotenv.2019.04.078

Vogelsang, C., Lusher, A., Dadkhah, M., Sundvor, I., Umar, M., Ranneklev, S., Eidsvoll, D., & Meland, S. (2018). Microplastics in road dust – characteristics, pathways and measures.

Volgare, M., Falco, F. D., Avolio, R., Castaldo, R., Errico, M. E., Gentile, G., Ambrogi, V., & Cocca, M. (2021). Washing load influences the microplastic release from polyester fabrics by affecting wettability and mechanical stress. *Scientific Reports*, *11*, 19479. https://doi.org/10.1038/s41598-021-98836-6

Wagner, W., & Kretzschmar, H.-J. (2008). *International steam tables*. Springer Berlin Heidelberg. https://doi.org/10.1007/978-3-540-74234-0

Waldschläger, K., & Schüttrumpf, H. (2019). Effects of particle properties on the settling and rise velocities of microplastics in freshwater under laboratory conditions. *Environmental Science & Technology*, *53*, 1958–1966. https://doi.org/10.1021/acs.est.8b06794

Wanders, N., van Vliet, M. T. H., Wada, Y., Bierkens, M. F. P., & van Beek, L. P. H. ((2019). High-resolution global water temperature modeling. *Water Resources Research*, *55*, 2760–2778. https://doi.org/10.1029/2018WR023250

Wang, C., Chen, W., Zhao, H., Tang, J., Li, G., Zhou, Q., Sun, J., & Xing, B. (2023). Microplastic fiber release by laundry: A comparative study of hand-washing and machine-washing. *ACS ES&T Water*, *3*, 147–155. https://doi.org/10.1021/acsestwater.2c00462

Yu, Z., Yang, G., & Zhang, W. (2022). A new model for the terminal settling velocity of microplastics. *Marine Pollution Bulletin*, *176*, 113449. https://doi.org/10.1016/j.marpolbul.2022.113449

Zong, C., Li, C., Zhu, L., Wang, X., Wei, N., Jiang, C., Dong, X., Jabeen, K., VO, T. T., & Li, D. (2024). Changes and transport of microplastics in the riverbed of the mainstream below the three gorges dam of the yangtze river. *Gondwana Research*, *128*, 340–350. https://doi.org/10.1016/j.gr.2023.11.005

Appendix A. Model repository

The GitHub repository for this project can be found here: https://github.com/arthurronner/Microplastic_Global_Transport_Model. Next to the washing machine ownership rate dataset,t his repository contains the code for the presented model, as well as the functions used to execute the model, the input data used, and data preparation functions. Additionally, the functions used to generate the final plots of this project can also be found in this repository. The output data for this project will be made available upon request.

Appendix B. Auxiliary calculations

B.1. Emissions calculation specifics

The relation between HDI and washing machine ownership rate is given in figure B.1. This relation was computed using a $k = 5$ nearest neighbor approximation with uniform weighting.

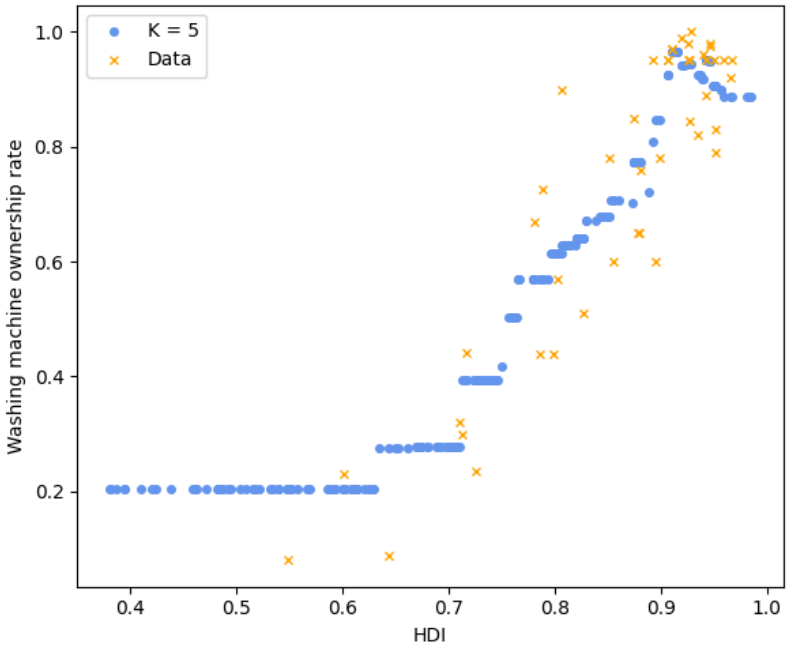

Figure B.1: Nearest neighbor ($k = 5$) approximation of washing machine ownership rates per country. Data from Laitala et al. (2018).

B.2. River length calculation

The river segment length was not present in the provided dataset, and was thus computed manually. To this end, the assumption was made that each river flows from the centre of its coordintates, to the centre of the adjacent cell to which it discharges. If the river segment does not discharge, we assume that it travels vertically to the edge of its own cell. As the input data uses latitudes and longitudes, we utilise an algorithm for calculating geodesic distance as introduced by Karney (2013). The code for this procedure can be found in the model repository (Appendix A).

Appendix C. Distribution functions for shape, density and size

Kooi and Koelmans (2019) derive an estimate for continuous distribution functions for particle size, shape, and density. These distributions were used to calculate the relative abundance of MPs within the same MP category in one mix (i.e. the relative occurrence between fiberA1, fiberA2, and fiberA3). Furthermore, they also derive upper an lower bounds for particle shape approximations (see figure C.1), which were used in this work to describe the different particles.

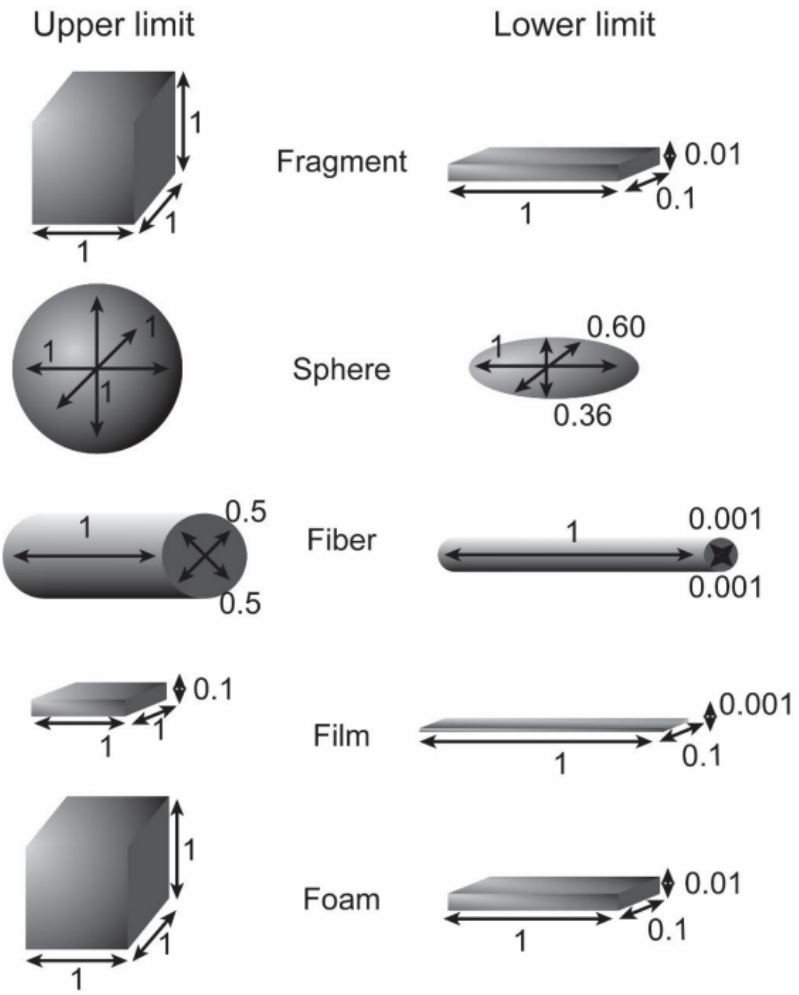

Figure C.1: Upper and lower boundaries for particle dimensions, per MP type. Bead particles correspond to the sphere category. Image obtained from Kooi and Koelmans (2019).

The distribution functions are given in equations C.1

$$y_{si} = \zeta a^{-\xi}, \qquad \zeta = (\xi - 1){a_{min}}^{\xi - 1} \qquad , \xi = 1.6, a_{min} = 20\mu\text{m} \tag{C.1a}$$

$$y_{sh} = \zeta_1 \frac{1}{\sqrt{2\pi\sigma_1^2}} \mathrm{e}^{-(CSF-\mu_1)^2/2\sigma_1^2} + \zeta_2 \frac{1}{\sqrt{2\pi\sigma_2^2}} \mathrm{e}^{-(CSF-\mu_2)^2/2\sigma_2^2} \tag{C.1b}$$

$$, \zeta_1 = 0.06, \sigma_1 = 0.03, \mu_1 = 0.08, \zeta_2 = 0.94, \sigma_2 = 0.19, \mu_2 = 0.44$$

$$y_\rho = \frac{\zeta_3 \delta K_1 \left[\zeta_3 \sqrt{\delta^2 + (\rho - \mu_3)^2}\right]}{\pi \sqrt{\delta^2 + (\rho - \mu_3)^2}} \mathrm{e}^{\delta\sqrt{\zeta_3^2 - \xi_3^2} + \xi_1(\rho - \mu_3)} \qquad , \zeta_3 = 75.1, \delta = 0.097, \mu_3 = 0.84, \xi_3 = 71.3 \tag{C.1c}$$

$$p = y_{si} y_{sh} y_\rho \tag{C.1d}$$

Where y_{si} (dependent on the particles a) is the particles size distribution value, log normally distributed. y_{sh} (dependent ont he particles CSF)is the particles shape distribution value, which is a combination of two normal distributions. y_ρ (dependent on the particles ρ) is the particles density distribution, which is normal-inverse Gaussian distributed. All $\zeta, \xi, \mu, \delta, \sigma, a_{min}$ values are distribution parameters that were fitted by Kooi and Koelmans (2019). K_1 is a modified Bessel function of the second kind (also called the third kind) with order 1. p is the resultant probability of the particle, which is compared against others of its type within its mix.

Appendix D. Wastewater treatement plant dataset

HydroWASTE (Macedo et al., 2022), a dataset on global WWTPs locations, filtering levels, and population served, was used in this project as a starting point for emission sources. The WWTP locations, as well as their population served, is given in figure D.1.

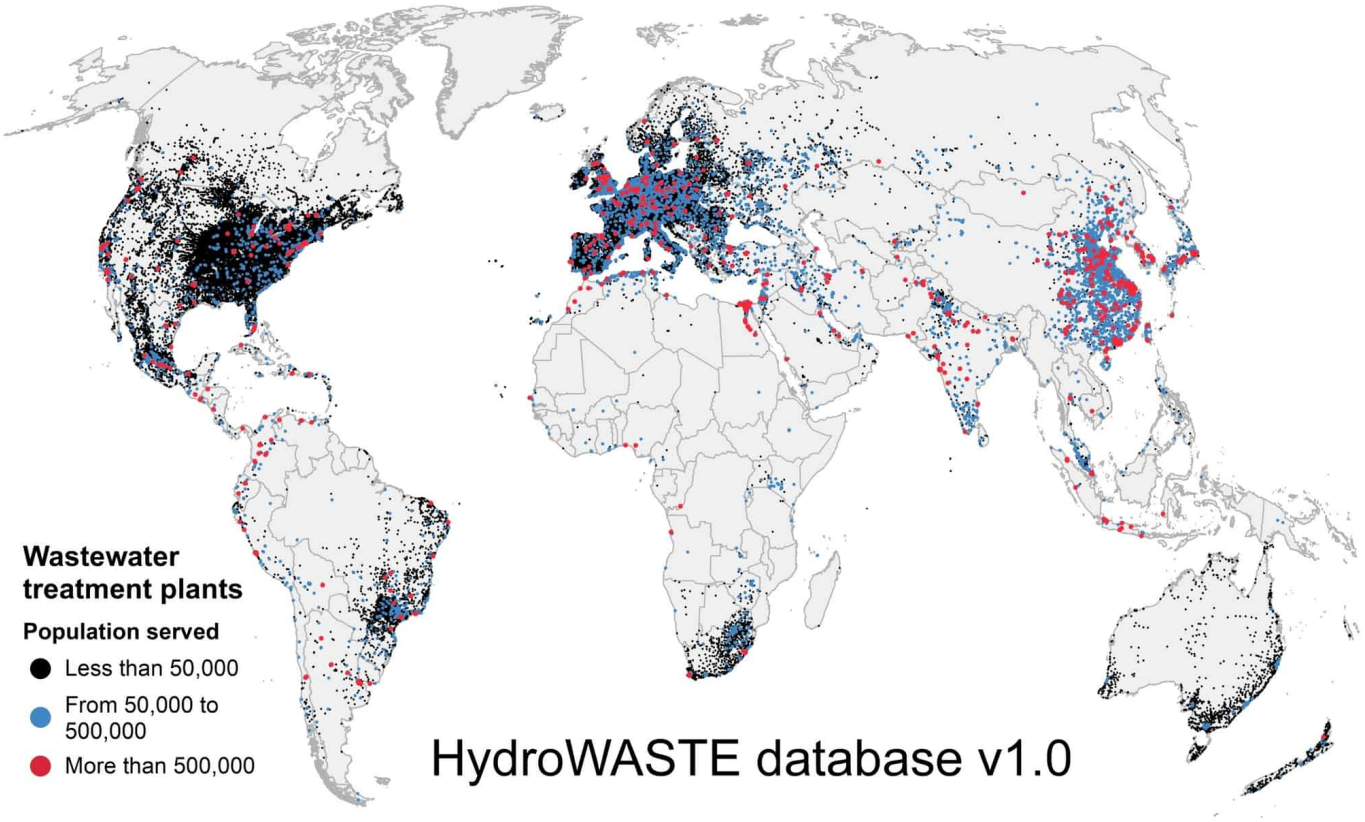

Figure D.1: Locations of WWTPs present in the HydroWASTE dataset. Image retrieved from Macedo et al. (2022).

Appendix E. Model matrix notation

Advection The methodology for advection is relatively well preserved. The globally applied formula is shown in equation E.2.

$$\mathbf{N_{MP,A}}(t) = \mathbf{Q}(t)t_s \odot \mathbf{N_{MPsus}}(t) \oslash \mathbf{V} \tag{E.2}$$

Where now the capital bold letters represent global 2160 $\times$ 4320 matrices, each element representing a grid cell. $\odot$ represents an elementwise product, and $\oslash$ represents an elementwise division. After the MP advection is calculated, $\mathbf{N_{MP,A}}(t)$ is subtracted from their respective river segment, and added to the destination segment using the input river direction map (Sutanudjaja et al., 2018). This is done by, for each direction (one for each adjacent cell), selecting the cells that discharge in that direction and adding their advected MP values to the target cells.

Settling As the river volume is calculated as that of a rectangular prism, we can rewrite and simplify formula 3 as follows for the whole globe.

$$\mathbf{N_{settle}} = \mathbf{U_s} \odot \mathbf{N_{MPsus}} \oslash \mathbf{H}t_s \tag{E.3}$$

Where the bold font capital letters represent matrix notation, and $\mathbf{H}$ (m) represents the river depth. $\mathbf{U_s}$ (m/s) is the particles settling velocity. Every timestep, $\mathbf{N_{settle}}$ is subtracted from the river suspended MP stocks, and added to the respective sediment MP stocks. All the underlying equations for $\mathbf{U_s}$ are given in equation E.4.

$$\mathbf{U_s} = \frac{2\sqrt{3}}{3}(g\mathbf{M}(T)\frac{\rho_s - \rho_f}{\rho_f})^{\circ\frac{1}{3}} \odot (\mathbf{D}_* \oslash \mathbf{C_d})^{\circ\frac{1}{2}} \tag{E.4a}$$

$$\mathbf{D}_* = (\frac{g(\rho_s - \rho_f)}{\rho_f})^{\circ\frac{1}{3}}\mathbf{M}(T)^{\circ-\frac{2}{3}}d_n, \tag{E.4b}$$

$$\mathbf{C_d} = \mathbf{C_{d,s}} \oslash \left(\mathbf{D_*}^{\circ\beta_1} \odot \psi^{\circ\mathbf{D_*}^{\circ\beta_2}} \odot CSF^{\circ\mathbf{D_*}^{\circ\beta_3}}\right)^{\circ\beta_4}, \tag{E.4c}$$

$$\begin{aligned}\mathbf{C_{d,s}} = {} & 432\mathbf{D_*}^{\circ-3} \odot \left(1 + 0.022\mathbf{D_*}^{\circ 3}\right)^{\circ 0.54} \\ & + 0.47\left(1 - \exp\left[-0.15\mathbf{D_*}^{\circ 0.45}\right]\right),\end{aligned} \tag{E.4d}$$

Where $\circ$ is an elementwise power. A constant to the power of a matrix (for instance $CSF^{\circ\mathbf{D}_*}$) implies that the constant CSF is filled to a 2160 $\times$ 4320 matrix, and subsequently an element power operation ($\circ$) is performed.

Entrainment The entrainment equations follow a similar alteration, though some equations, like equation E.5f are further simplified compared to their single segment counterpart.

$$\mathbf{N_{ent}} = \gamma_8\mathbf{N_{MPsed}} \odot \mathbf{P_{prop}} \odot \mathbf{\Omega} \odot \mathbf{F} \tag{E.5a}$$

$$\mathbf{P_{prop}} = \min(\max(\frac{\mathbf{A_{max}} - a_{low}}{a_{upp} - a_{low}}, 0), 1) \tag{E.5b}$$

$$\mathbf{A_{max}} = 9.9941(\mathbf{U}^*)^{\circ 2.5208} \tag{E.5c}$$

$$\mathbf{U}^* = (g\gamma_7\mathbf{H} \odot \mathbf{S})^{\circ\frac{1}{2}} \tag{E.5d}$$

$$\mathbf{\Omega} = g\rho_f\mathbf{Q} \odot \mathbf{S} \oslash (\mathbf{W} \odot \mathbf{H}) \tag{E.5e}$$

$$\mathbf{F} = 4\mathbf{H} \oslash (2\mathbf{H} + \mathbf{W}) \tag{E.5f}$$

Where $\mathbf{A_{max}}$ (m) is the MPs largest dimension, $\mathbf{F}$ is the friction factor, and $\mathbf{U}^*$ (m/s) is the river shear velocity.

Appendix F. Model performance

This work was performed using the compute resources from the Academic Leiden Interdisciplinary Cluster Environment (ALICE) provided by Leiden University. Specifically, for one MP mix, one node, 12 cores, and 28 Gb of RAM was used to run all 24 model runs in parallel. The computation time on ALICE varied greatly between nodes (which might depend on other tasks), between roughly 2-4 days. It should be noted that running smaller batches of runs, with more allocated memory, can result in faster model runtime (to about 1.5 days for 18 runs on 9 cores, 32 Gb each).

Appendix G. Generated samples and mixes

This appendix contains the samples and MP mixes as used in the presented model runs. The uncertainty samples, generated using table 3, are presented in table G.1. The different generated MP mixes, from the parameter ranges represented in 2, are presented in tables G.2-G.9.

Table G.1: Full samples as generated from the ranges presented in table 3

	γ_7	γ_8 $\times 10^{-6}$ (s^2kg^{-1})	β_1	β_2	β_3	β_4	$r_{eff,P}$	$r_{eff,S}$	$r_{eff,A}$	$N_{MP,wash}$	p_{MPfib}	p_{MPfra}	p_{MPfil}	p_{MPb}	p_{MPfo}
0	0.0703	3.35	−0.321	−0.277	0.48	0.223	0.84	0.961	0.99	5.75×10^5	0.656	0.236	0.0694	0.000 321	0.038
1	0.0424	0.696	−0.159	0.298	0.231	0.298	0.78	0.965	0.993	1.45×10^6	0.47	0.301	0.122	0.0767	0.031
2	0.0497	1.79	−0.207	0.318	0.374	0.144	0.871	0.957	0.993	1.09×10^6	0.577	0.298	0.0592	0.0386	0.0271
3	0.0281	2.73	−0.282	−0.173	0.474	0.238	0.767	0.95	0.987	1.42×10^6	0.521	0.317	0.0791	0.0464	0.0359
4	0.0267	0.848	−0.217	−0.0301	0.189	0.334	0.879	0.962	0.989	7.28×10^5	0.456	0.341	0.105	0.0785	0.0193
5	0.0077	2.01	−0.186	0.269	0.182	0.295	0.81	0.945	0.988	9.63×10^5	0.458	0.353	0.0915	0.0813	0.0164
6	0.0736	0.335	−0.297	0.208	0.218	0.189	0.818	0.946	0.992	8.32×10^5	0.581	0.223	0.109	0.0386	0.048
7	0.033	1.11	−0.253	−0.144	0.25	0.168	0.82	0.949	0.988	1.36×10^6	0.681	0.13	0.106	0.0661	0.0172
8	0.0683	1.71	−0.131	−0.0709	0.266	0.261	0.848	0.954	0.995	1.2×10^6	0.401	0.433	0.0981	0.0169	0.0512
9	0.0592	1.4	−0.192	−0.116	0.294	0.212	0.854	0.938	0.993	8.7×10^5	0.42	0.376	0.129	0.0447	0.0308
10	0.0197	2.45	−0.228	−0.247	0.204	0.286	0.834	0.948	0.991	1.31×10^6	0.404	0.288	0.187	0.0908	0.0307
11	0.0617	0.413	−0.146	−0.311	0.404	0.364	0.827	0.964	0.989	6.21×10^5	0.555	0.295	0.124	0.006 38	0.0198
12	0.0514	1.49	−0.355	−0.284	0.16	0.308	0.806	0.942	0.994	1.19×10^6	0.625	0.126	0.129	0.0741	0.0464
13	0.0157	2.82	−0.2	−0.209	0.433	0.174	0.862	0.944	0.991	1.04×10^6	0.541	0.34	0.0677	0.0272	0.0235
14	0.006 57	2.97	−0.152	0.005 13	0.329	0.224	0.859	0.952	0.989	7.76×10^5	0.507	0.222	0.147	0.0627	0.0608
15	0.0437	3.87	−0.33	0.386	0.298	0.126	0.872	0.955	0.99	1.38×10^6	0.514	0.255	0.122	0.0552	0.0536
16	0.0534	3.09	−0.267	0.115	0.318	0.343	0.776	0.941	0.99	5.03×10^5	0.629	0.253	0.0646	0.0188	0.0346
17	0.0334	0.544	−0.239	0.0436	0.454	0.135	0.788	0.939	0.995	1.27×10^6	0.426	0.276	0.155	0.107	0.0359
18	0.0636	3.75	−0.345	0.351	0.346	0.276	0.832	0.959	0.991	1.01×10^6	0.369	0.422	0.0703	0.0977	0.0407
19	0.0208	3.55	−0.341	0.239	0.441	0.197	0.847	0.963	0.994	6.69×10^5	0.61	0.272	0.0906	0.006 64	0.0205
20	0.0119	2.32	−0.309	0.124	0.388	0.351	0.79	0.951	0.987	1.14×10^6	0.65	0.182	0.0925	0.0258	0.0504
21	0.003 12	3.4	−0.172	0.0669	0.412	0.327	0.795	0.946	0.995	5.38×10^5	0.526	0.251	0.128	0.025	0.0697
22	0.0387	1.22	−0.264	−0.0515	0.356	0.159	0.783	0.956	0.992	9.07×10^5	0.689	0.119	0.0988	0.0539	0.0396
23	0.0769	2.22	−0.29	0.181	0.278	0.246	0.803	0.958	0.993	6.8×10^5	0.668	0.179	0.0885	0.0343	0.0307

Table G.2: Microplastic mix 1

Names	ρ_s (kg)	a_{low} (mm)	a (mm)	a_{upp} (mm)	b (mm)	c (mm)	CSF	ψ	V_p ($\times 10^{-3}$ mm^3)	Occurrence
fiberA1	1037	0.644	0.716	0.787	0.0607	0.0607	0.291	0.552	2.07	0.197
fiberA2	1141	0.404	0.449	0.494	0.184	0.184	0.64	0.808	11.9	0.286
fiberA3	1283	0.286	0.317	0.349	0.0749	0.0749	0.486	0.724	1.4	0.517
fragmentA1	1271	0.687	0.764	0.84	0.233	0.206	0.489	0.696	36.6	0.0926
fragmentA2	1615	0.523	0.582	0.64	0.442	0.16	0.316	0.685	41.2	0.0273
fragmentA3	1159	0.217	0.242	0.266	0.167	0.0942	0.469	0.747	3.81	0.88
foamA1	1127	0.475	0.528	0.581	0.151	0.0785	0.278	0.617	6.27	0.0386
foamA2	1108	0.0629	0.0699	0.0769	0.0476	0.0357	0.619	0.777	0.119	0.946
foamA3	1019	0.762	0.847	0.931	0.607	0.164	0.229	0.618	84.4	0.0151
beadA1	1218	0.528	0.587	0.646	0.389	0.224	0.468	0.884	214	0.759
beadA2	1631	0.323	0.359	0.395	0.264	0.259	0.842	0.983	103	0.031
beadA3	1359	0.686	0.762	0.839	0.741	0.446	0.593	0.949	1.05×10^3	0.21
filmA1	1073	0.784	0.871	0.958	0.523	0.0424	0.0628	0.338	19.3	0.646
filmA2	1512	0.395	0.439	0.483	0.364	0.014	0.0351	0.242	2.25	0.193
filmA3	1609	0.275	0.305	0.336	0.0647	0.003 54	0.0252	0.195	0.07	0.161

Table G.3: Microplastic mix 2

Names	ρ_s (kg)	a_{low} (mm)	a (mm)	a_{upp} (mm)	b (mm)	c (mm)	CSF	ψ	V_p ($\times 10^{-3}$ mm^3)	Occurrence
fiberB1	1239	0.734	0.816	0.898	0.231	0.231	0.532	0.754	34.2	0.153
fiberB2	1028	0.306	0.34	0.374	0.15	0.15	0.665	0.817	6.01	0.538
fiberB3	1133	0.541	0.601	0.661	0.0567	0.0567	0.307	0.57	1.52	0.309
fragmentB1	1267	0.173	0.192	0.212	0.0572	0.055	0.525	0.7	0.605	0.959
fragmentB2	1513	0.736	0.818	0.9	0.489	0.111	0.175	0.555	44.2	0.014
fragmentB3	1745	0.457	0.508	0.559	0.461	0.235	0.485	0.757	55	0.0272
foamB1	1114	0.148	0.165	0.181	0.12	0.12	0.85	0.797	2.37	0.26
foamB2	1132	0.751	0.834	0.918	0.303	0.0526	0.105	0.434	13.3	0.0957
foamB3	1033	0.374	0.416	0.458	0.273	0.154	0.458	0.742	17.6	0.644
beadB1	1224	0.864	0.96	1.06	0.671	0.61	0.76	0.972	1.65×10^3	0.0957
beadB2	1460	0.148	0.164	0.18	0.163	0.121	0.742	0.984	13.6	0.718
beadB3	1718	0.367	0.408	0.449	0.307	0.16	0.453	0.881	83.9	0.186
filmB1	1690	0.87	0.967	1.06	0.783	0.0344	0.0395	0.26	26	0.0226
filmB2	1362	0.384	0.427	0.469	0.19	0.0147	0.0516	0.301	1.19	0.502
filmB3	1110	0.275	0.306	0.337	0.036	0.000 41	0.003 95	0.0596	0.004 57	0.476

Table G.4: Microplastic mix 3

Names	ρ_s (kg)	a_{low} (mm)	a (mm)	a_{upp} (mm)	b (mm)	c (mm)	CSF	ψ	V_p ($\times 10^{-3}$ mm^3)	Occurrence
fiberC1	1029	0.609	0.677	0.745	0.255	0.255	0.614	0.796	34.6	0.0119
fiberC2	1140	0.0456	0.0507	0.0558	0.0075	0.0075	0.385	0.645	0.002 24	0.979
fiberC3	1223	0.646	0.718	0.79	0.225	0.225	0.56	0.77	28.6	0.009 25
fragmentC1	1298	0.0908	0.101	0.111	0.0338	0.0271	0.463	0.7	0.0924	0.93
fragmentC2	1168	0.706	0.784	0.863	0.583	0.325	0.48	0.752	148	0.055
fragmentC3	1610	0.35	0.389	0.428	0.249	0.0311	0.1	0.432	3.02	0.0147
foamC1	1145	0.48	0.533	0.586	0.0857	0.0141	0.0661	0.332	0.645	0.152
foamC2	1114	0.64	0.712	0.783	0.566	0.446	0.703	0.791	179	0.0781
foamC3	1034	0.289	0.321	0.353	0.222	0.116	0.435	0.737	8.3	0.77
beadC1	1724	0.0647	0.0719	0.0791	0.0494	0.0433	0.727	0.966	0.644	0.511
beadC2	1351	0.355	0.394	0.434	0.308	0.25	0.716	0.973	127	0.189
beadC3	1088	0.86	0.955	1.05	0.936	0.475	0.503	0.913	1.78×10^3	0.3
filmC1	1611	0.39	0.433	0.476	0.424	0.0194	0.0452	0.281	3.56	0.162
filmC2	1482	0.209	0.232	0.256	0.0373	0.0037	0.0397	0.252	0.032	0.659
filmC3	1234	0.718	0.798	0.878	0.439	0.0171	0.0289	0.215	5.98	0.179

Table G.5: Microplastic mix 4

Names	ρ_s (kg)	a_{low} (mm)	a (mm)	a_{upp} (mm)	b (mm)	c (mm)	CSF	ψ	V_p ($\times 10^{-3}$ mm^3)	Occurrence
fiberD1	1073	0.502	0.558	0.613	0.17	0.17	0.552	0.765	12.6	0.122
fiberD2	1135	0.755	0.839	0.923	0.0224	0.0224	0.164	0.387	0.332	0.0241
fiberD3	1255	0.0796	0.0885	0.0973	0.0386	0.0386	0.66	0.816	0.103	0.854
fragmentD1	1308	0.648	0.72	0.792	0.355	0.0678	0.134	0.493	17.3	0.0325
fragmentD2	1125	0.222	0.247	0.272	0.217	0.102	0.441	0.744	5.49	0.951
fragmentD3	1734	0.552	0.613	0.674	0.19	0.181	0.531	0.705	21.1	0.0163
foamD1	1092	0.638	0.709	0.78	0.178	0.0286	0.0803	0.375	3.61	0.189
foamD2	1168	0.0865	0.0961	0.106	0.08	0.0776	0.885	0.802	0.597	0.435
foamD3	1032	0.526	0.584	0.643	0.333	0.141	0.32	0.679	27.4	0.377
beadD1	1650	0.251	0.279	0.307	0.27	0.166	0.605	0.953	52.3	0.324
beadD2	1471	0.346	0.384	0.423	0.257	0.143	0.455	0.877	59	0.627
beadD3	1058	0.864	0.96	1.06	0.802	0.758	0.864	0.992	2.44×10^3	0.0493
filmD1	1575	0.702	0.78	0.858	0.124	0.0041	0.0132	0.13	0.397	0.001 69
filmD2	1282	0.606	0.673	0.74	0.494	0.0336	0.0583	0.325	11.2	0.0295
filmD3	1003	0.0848	0.0942	0.104	0.0465	0.0033	0.0499	0.296	0.0145	0.969

Table G.6: Microplastic mix 5

Names	ρ_s (kg)	a_{low} (mm)	a (mm)	a_{upp} (mm)	b (mm)	c (mm)	CSF	ψ	V_p ($\times 10^{-3}$ mm^3)	Occurrence
fiberE1	1278	0.777	0.863	0.949	0.273	0.273	0.562	0.771	50.3	0.0418
fiberE2	1049	0.172	0.191	0.21	0.0719	0.0719	0.614	0.796	0.775	0.689
fiberE3	1118	0.366	0.407	0.448	0.0563	0.0563	0.372	0.634	1.01	0.27
fragmentE1	1711	0.732	0.814	0.895	0.179	0.0988	0.259	0.587	14.4	0.0402
fragmentE2	1529	0.325	0.361	0.397	0.334	0.103	0.298	0.676	12.5	0.395
fragmentE3	1268	0.585	0.65	0.715	0.277	0.221	0.521	0.732	39.9	0.564
foamE1	1133	0.176	0.195	0.215	0.101	0.0729	0.52	0.745	1.44	0.832
foamE2	1045	0.838	0.931	1.02	0.713	0.281	0.345	0.701	187	0.0739
foamE3	1112	0.417	0.464	0.51	0.0596	0.03	0.18	0.492	0.829	0.0943
beadE1	1568	0.085	0.0944	0.104	0.0596	0.0557	0.742	0.961	1.31	0.532
beadE2	1449	0.517	0.575	0.632	0.464	0.353	0.684	0.968	394	0.0782
beadE3	1082	0.705	0.784	0.862	0.702	0.353	0.477	0.899	814	0.39
filmE1	1243	0.89	0.989	1.09	0.608	0.0347	0.0448	0.279	20.9	0.23
filmE2	1490	0.476	0.529	0.582	0.106	0.001 46	0.006 17	0.08	0.0821	0.0656
filmE3	1623	0.208	0.231	0.254	0.169	0.0124	0.0626	0.338	0.482	0.704

Table G.7: Microplastic mix 6

Names	ρ_s (kg)	a_{low} (mm)	a (mm)	a_{upp} (mm)	b (mm)	c (mm)	CSF	ψ	V_p ($\times 10^{-3}$ mm^3)	Occurrence
fiberF1	1200	0.579	0.643	0.707	0.0685	0.0685	0.326	0.59	2.37	0.16
fiberF2	1131	0.239	0.266	0.292	0.0851	0.0851	0.566	0.773	1.51	0.776
fiberF3	1084	0.876	0.973	1.07	0.438	0.438	0.671	0.82	147	0.0632
fragmentF1	1263	0.28	0.311	0.342	0.246	0.138	0.497	0.758	10.5	0.764
fragmentF2	1660	0.881	0.979	1.08	0.495	0.101	0.145	0.511	49	0.007 77
fragmentF3	1366	0.471	0.524	0.576	0.153	0.125	0.444	0.682	10	0.229
foamF1	1011	0.153	0.17	0.188	0.0278	0.0179	0.26	0.564	0.0851	0.91
foamF2	1160	0.597	0.664	0.73	0.532	0.51	0.859	0.801	180	0.0124
foamF3	1099	0.668	0.742	0.817	0.431	0.135	0.238	0.622	43.1	0.0775
beadF1	1750	0.855	0.95	1.04	0.855	0.623	0.691	0.974	2.12×10^3	0.000 609
beadF2	1154	0.0614	0.0682	0.075	0.0544	0.0337	0.554	0.931	0.524	0.998
beadF3	1537	0.563	0.626	0.688	0.4	0.381	0.76	0.964	399	0.001 79
filmF1	1380	0.857	0.952	1.05	0.489	0.0355	0.0521	0.304	16.5	0.165
filmF2	1031	0.402	0.447	0.491	0.0805	0.004 96	0.0262	0.199	0.179	0.684
filmF3	1713	0.263	0.292	0.321	0.241	0.009 24	0.0349	0.241	0.65	0.151

Table G.8: Microplastic mix 7

Names	ρ_s (kg)	a_{low} (mm)	a (mm)	a_{upp} (mm)	b (mm)	c (mm)	CSF	ψ	V_p ($\times 10^{-3}$ mm^3)	Occurrence
fiberG1	1190	0.58	0.644	0.708	0.0554	0.0554	0.293	0.555	1.55	0.0252
fiberG2	1205	0.646	0.718	0.79	0.35	0.35	0.699	0.829	69.2	0.0107
fiberG3	1008	0.0822	0.0913	0.1	0.018	0.018	0.444	0.694	0.0232	0.964
fragmentG1	1443	0.34	0.378	0.416	0.115	0.016	0.0768	0.37	0.696	0.378
fragmentG2	1210	0.846	0.94	1.03	0.567	0.34	0.465	0.74	181	0.399
fragmentG3	1574	0.231	0.257	0.282	0.194	0.162	0.728	0.792	8.08	0.223
foamG1	1001	0.607	0.674	0.742	0.452	0.45	0.815	0.792	137	0.025
foamG2	1173	0.154	0.171	0.188	0.0378	0.0215	0.267	0.592	0.139	0.902
foamG3	1117	0.745	0.828	0.91	0.8	0.195	0.24	0.631	129	0.0727
beadG1	1244	0.809	0.899	0.989	0.785	0.752	0.895	0.995	2.22×10^3	0.006 93
beadG2	1617	0.407	0.452	0.497	0.288	0.189	0.523	0.907	103	0.0681
beadG3	1364	0.146	0.163	0.179	0.135	0.0844	0.57	0.938	7.75	0.925
filmG1	1322	0.82	0.912	1	0.484	0.042	0.0632	0.339	18.5	0.18
filmG2	1573	0.153	0.17	0.187	0.0378	0.000 89	0.011	0.117	0.0057	0.195
filmG3	1157	0.422	0.469	0.515	0.468	0.0211	0.0451	0.281	4.63	0.625

Table G.9: Microplastic mix 8

Names	ρ_s (kg)	a_{low} (mm)	a (mm)	a_{upp} (mm)	b (mm)	c (mm)	CSF	ψ	V_p ($\times 10^{-3}$ mm^3)	Occurrence
fiberH1	1175	0.836	0.929	1.02	0.441	0.441	0.689	0.826	142	0.0727
fiberH2	1281	0.272	0.302	0.332	0.0775	0.0775	0.507	0.738	1.42	0.666
fiberH3	1009	0.367	0.408	0.449	0.009 68	0.009 68	0.154	0.372	0.03	0.261
fragmentH1	1136	0.224	0.249	0.274	0.0452	0.0271	0.255	0.57	0.306	0.911
fragmentH2	1597	0.761	0.846	0.93	0.748	0.629	0.791	0.8	398	0.005 91
fragmentH3	1412	0.49	0.545	0.599	0.243	0.0853	0.234	0.61	11.3	0.0829
foamH1	1164	0.0478	0.0532	0.0585	0.018	0.0147	0.476	0.704	0.0141	0.975
foamH2	1020	0.705	0.783	0.862	0.617	0.362	0.52	0.764	175	0.0145
foamH3	1096	0.461	0.512	0.563	0.358	0.0656	0.153	0.528	12	0.0106
beadH1	1031	0.328	0.364	0.401	0.286	0.227	0.702	0.971	98.9	0.647
beadH2	1783	0.786	0.873	0.961	0.601	0.509	0.703	0.962	1.12×10^3	0.009 69
beadH3	1274	0.576	0.64	0.705	0.565	0.318	0.528	0.923	482	0.343
filmH1	1528	0.517	0.574	0.631	0.169	0.0126	0.0403	0.259	1.22	0.158
filmH2	1204	0.85	0.945	1.04	0.548	0.0099	0.0138	0.135	5.12	0.114
filmH3	1561	0.192	0.214	0.235	0.185	0.008 62	0.0433	0.274	0.341	0.728